OPEN

NPG Asia Materials (2015) 7, e179; doi:10.1038/am.2015.27

www.nature.com/am

REVIEW

CeO_2-encapsulated noble metal nanocatalysts: enhanced activity and stability for catalytic application

Shuyan Song, Xiao Wang and Hongjie Zhang

Encapsulation of small noble metal nanoparticles has received attention owing to the resulting highly increased stability and high catalytic activity and selectivity. Among the types of inert metal oxides, CeO_2 is unique. It is inexpensive and highly stable, and, more importantly, the unique electronic configuration gives it a strong capability to provide active oxygen. The method of fabricating CeO_2-encapsulated noble metal nanocatalysts is determined by the requirements of the application. In this review, we first describe the various types of encapsulated noble metals and then the current developments of synthesis in detail, including the types of hybrid nanostructures and successful synthetic strategies. The following section, concerning catalytic applications, is divided into three topics: anti-sintering capabilities, catalytic activities and selectivities. We hope that this review of the recent achievements and the proposed strategy for addressing the emerging challenges will inspire further developments in this research area.
NPG Asia Materials (2015) **7,** e179; doi:10.1038/am.2015.27; published online 8 May 2015

INTRODUCTION

Noble metal catalysts have received much attention in the past decade because of their unique chemical and physical properties, and they have been widely applied in industrial use.[1–10] With the help of noble metal catalysts, environmental friendly catalysis resulting in the decreased production of pollutants, waste minimization and new synthetic routes that circumvent modern synthetic techniques such as Sonogashira–, Heck– and Miyaura–Suzuki-type reactions can be easily realized.[11–15] However, for most technologically important chemical processes, noble metal catalysts spontaneously aggregate and grow to reduce the surface energy, which limits the catalysts' lifetime and efficiency. The ultra-high prices of noble metals have also seriously limited their further development. Because of the development of modern industry, there remains a critical need for robust, simple and readily controllable routes to fabricate highly active, stable and recyclable nanocatalysts.

To maximize the catalytic performance of noble metals and reduce the quantity used, it is necessary to load the active centers on a substrate.[16–20] A suitable substrate not only provides a high surface area to stabilize small nanoparticles (NPs) under long-term catalysis but also renders hybrid junctions with rich redox reactions on the two-phase interface. With the development of synthetic techniques in nanoscience, small noble metal NPs, especially atomically precise nanoclusters/metal oxide hybrid nanostructures, have been successfully fabricated very recently, and these materials exhibit remarkable enhanced catalytic activity and selectivity.[21–23] However, this simple loading form cannot meet the growing demand for the stability, because the noble metal catalysts contain numerous exposed surfaces and are always used in harsh environments, such as those with high temperatures and concentrated acid and alkali solutions. The lack of surface protection causes the noble metal NPs to easily aggregate to minimize the surface energy, which can cause a serious loss of the catalytic active sites, a reduction of the catalytic activity and even complete inactivation (as shown in Scheme 1). Therefore, determining how to improve the stability of the noble metal catalysts is one of the most important problems in current nanoscience.

The concept of 'encapsulation' emerged with the aim of substantially increasing the stability of noble metals. Embedding small noble

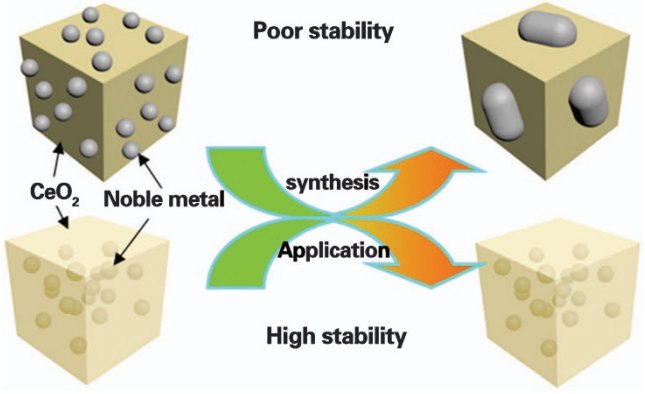

Scheme 1 Schematic representation of the different stabilities of noble metal-CeO_2 simple loading form and CeO_2 encapsulated noble metal nanostructures under long-term synthetic or catalytic processes.

State Key Laboratory of Rare Earth Resource Utilization, Changchun Institute of Applied Chemistry, Chinese Academy of Sciences, Changchun, P.R. China
Correspondence: Professor H Zhang, State Key Laboratory of Rare Earth Resource Utilization, Changchun Institute of Applied Chemistry, Chinese Academy of Sciences, Renmin Street 5625, Changchun 130022, P.R. China.
E-mail: hongjie@ciac.ac.cn
Received 16 October 2014; revised 20 January 2015; accepted 9 February 2015

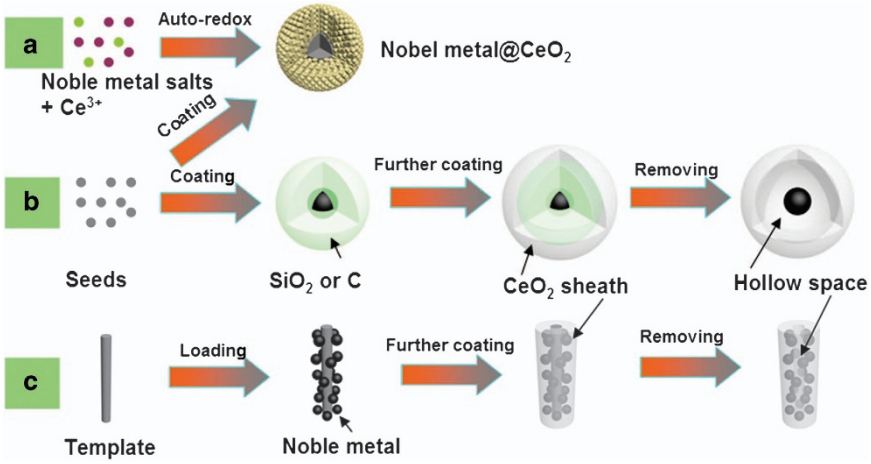

Scheme 2 Schematic representation of the three methods for the synthesis of CeO_2-encapsulated noble metal nanostructures: (**a**) auto-redox reaction, (**b**) seeded growth method, and (**c**) hard template strategy.

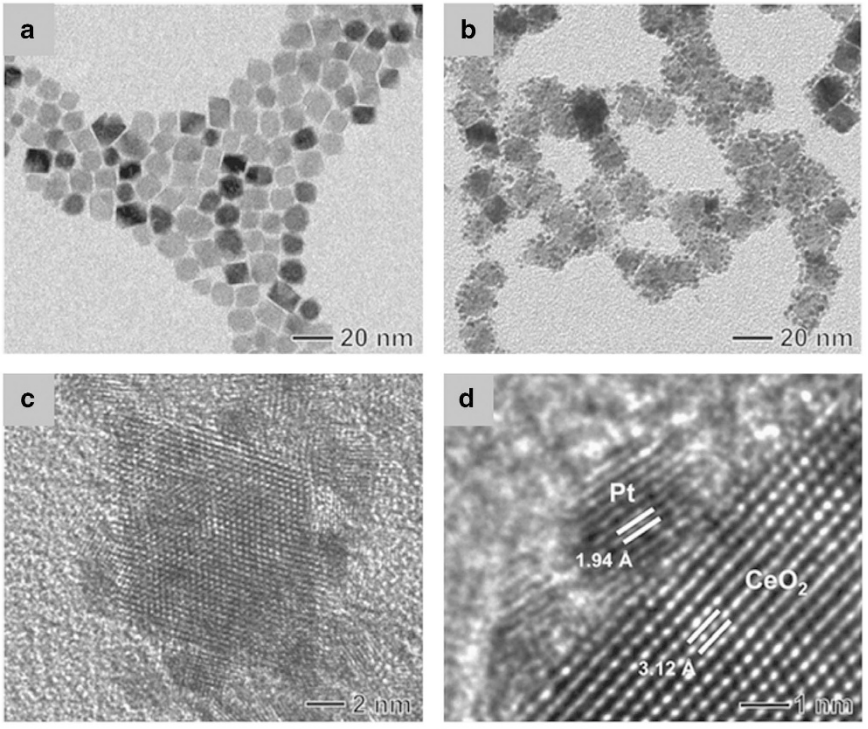

Table 1. Zeta potential values of AHA-stabilized CeO_2 octahedra, PVP-stabilized CeO_2 octahedra, Pt/CeO_2 hybrid nanostructures, and PVP-stabilized Pt nanocrystals at pH ≈ 5.5.

	Stabilizer	Zeta Potential [mV]
CeO_2 octahedra	AHA	+48.4
	PVP	+0.6
Pt/CeO_2 nanostructures	AHA and PVP	−1.1
Pt nanocrystals	PVP	−6.7

Figure 1 TEM images of CeO_2 octahedral stabilized by AHA (**a**) and Pt–CeO_2 hybrid nanostructures (**b**); HR TEM images of the Pt–CeO_2 (**c**) and (**d**). Reprinted with permission from Yu *et al.*[76] Copyright 2010 Wiley-VCH.

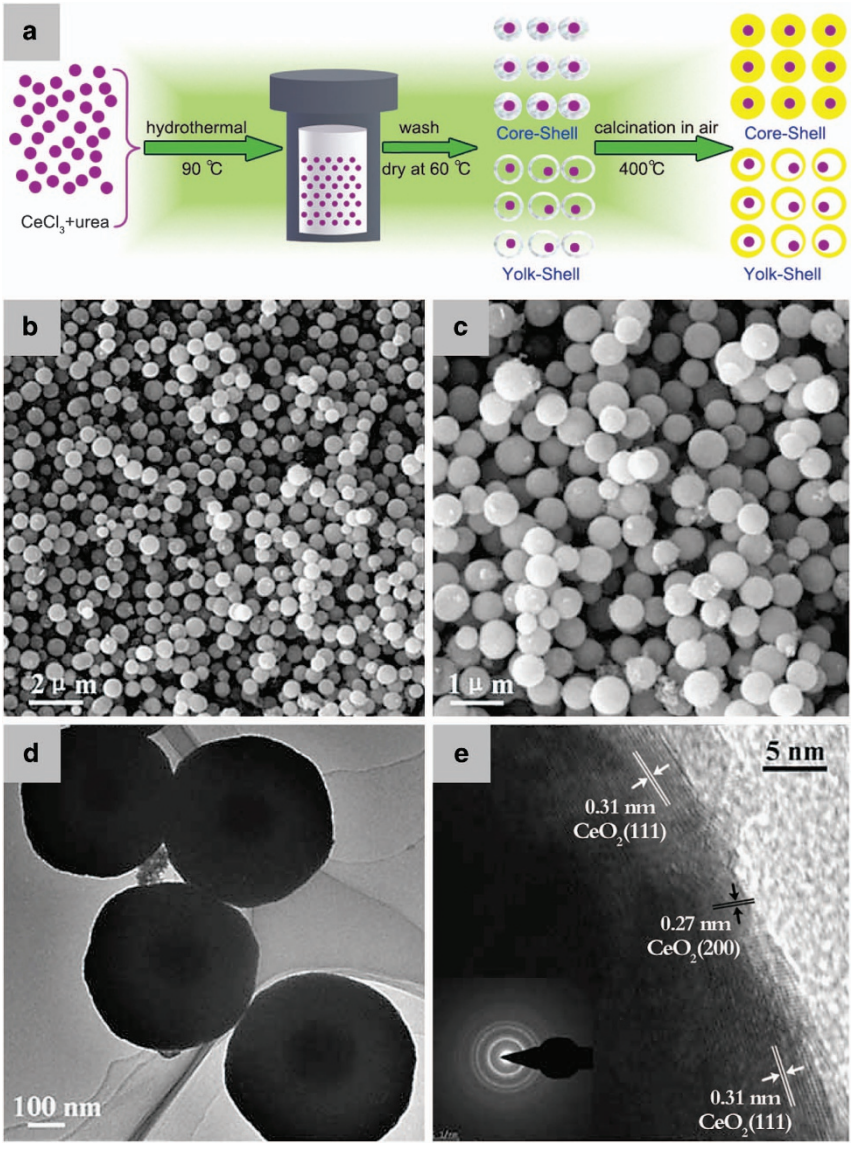

Figure 2 (**a**) Schematic representation of the synthesis of the Pt@CeO_2 core–shell or yolk–shell nanostructures via a hydrothermal method; (**b** and **c**) SEM images of Pt@CeO_2 core–shell NPs; (**d**) TEM image of Pt@CeO_2 core–shell NPs; and (**e**) high-resolution TEM image of Pt@CeO_2 core–shell NPs. Reprinted with permission from Zhang *et al.*[77] Copyright 2011 Royal Society of Chemistry.

metal NPs into highly stable porous inorganic nanostructures (for example, CeO_2,[24–26] TiO_2,[27–34] SiO_2,[35–39] ZrO_2[40,41]) and encapsulating noble metal NPs within metal oxides to form core–shell or yolk–shell nanostructures are common strategies. Three requirements must be satisfied simultaneously: (1) the sheath must maintain its chemical inertness in the specific working environment; (2) mass transformation must be avoided during the long-term synthetic and catalytic process, especially under high-temperature treatment; (3) after heat treatment, the active sites should maintain their original particle size, shape and catalytic activities.

Of the various shell materials, including SiO_2, TiO_2, SnO_2, ZrO_2 and CeO_2, CeO_2 clearly has the broadest spectrum of applicability. Cerium (Ce) is one of the most abundant elements and is much more abundant in the Earth's crust (66.5 p.p.m.) than even copper (60 p.p.m.) or tin (2.3 p.p.m.). Because of its unique electronic configuration ([Xe] $4f^26s^2$), Ce has two common valence states—Ce^{3+} and Ce^{4+}—which give CeO_2 excellent chemical and physical properties: 1/4 O_2, at most, can be released from each CeO_2 unit cell.[42] It serves as an active oxygen donor in many reactions, such as three-way catalytic reactions to eliminate toxic automobile exhaust,[43] the low-temperature water–gas shift reaction,[44,45] oxygen sensors,[46–48] oxygen permeation membrane systems[49] and fuel cells.[50–56] Furthermore, the growth process of CeO_2 NPs is easily controlled such that they can maintain their small particle sizes and uniform morphologies, key features in the coating process. Many types of CeO_2-encapsulated noble metal superstructures have been successfully prepared. There are five types of typical hybrid nanostructures: (1) core–shell hybrid nanostructures, composed of one or more cores uniformly coated with a dense CeO_2 layer; (2) yolk–shell or rattle-type hybrid nanostructures, that is, a single movable noble metal core inside a hollow CeO_2 sheath; (3) hollow multi-core-shell structures, composed of many noble metal NPs encapsulated within a CeO_2 hollow sheath; (4) sandwich structures, so-called for their interlayers composed of multiple noble metal NPs embedded in a CeO_2 film; and (5) multiple noble metal NPs

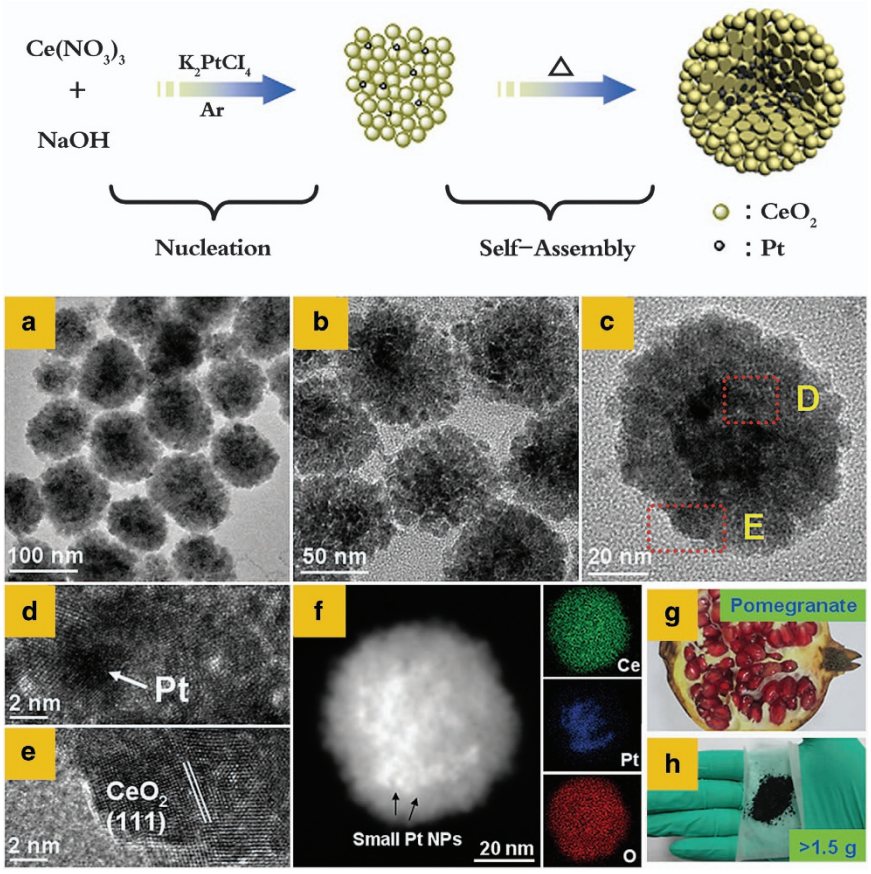

Figure 3 (**a**) Schematic representation of the synthesis of the Pt@CeO_2 multi-core–shell nanostructures via an auto-redox reaction; (**b**–**d**) TEM, (**e** and **f**) HR-TEM and STEM images of the as-prepared Pt@CeO_2 multi-core–shell hybrid nanostructures; (**g**) interior of a real pomegranate; (**h**) products obtained in one pot. Reprinted with permission from Wang *et al*.[78] Copyright 2013 American Chemical Society.

embedded within a porous CeO_2 matrix. However, it is not possible to cover all aspects of these categories and cite the relevant references in one article. In this review, we first summarize the preparation of CeO_2-encapsulated noble metal nanocatalysts. The following section, on catalytic applications, is divided into three topics: anti-sintering capabilities, catalytic activities and selectivity. In this section, we discuss the influence of the hybrid nanostructure on the catalytic performance. Finally, we describe the emerging challenges and future developments of CeO_2-based noble metal nanocatalysts.

SYNTHESIS OF CEO_2-ENCAPSULATED NOBLE METAL NANOCATALYSTS WITH VARIOUS MORPHOLOGIES

Very recently, many synthetic strategies have been successfully developed to prepare noble metal–CeO_2 hybrid nanocatalysts.[57–63] Generally, the methods used for the synthesis of CeO_2-encapsulated noble metal nanocatalysts can be divided into three categories (as shown in Scheme 2): one-pot synthesis, multi-step layer-by-layer coating processes and hard-template methods. Unlike other common shell components with continuous phases, including SiO_2,[35–39] TiO_2,[27–34] SnO_2,[64–66] Cu_2O,[67–72] ZnO[73] and ZrO_2,[40,41] the CeO_2 layer is composed of hundreds of tiny CeO_2 NPs assembled together instead of a single continuous crystal. Therefore, it is believed that, of the various experimental parameters, including reaction temperature, time, surface state of the noble metal seeds and solvent pH value, the most important characteristic is how the independent nucleation of the CeO_2 NPs is controlled. Many types of CeO_2-encapsulated noble metal superstructures, such as Pt@CeO_2, Pd@CeO_2, Au@CeO_2 and Ag@CeO_2, have been successfully synthesized. However, for other noble metals, such as Ru, Ir, Rh and multi-component noble metal alloys, a similar hybrid nanostructure has yet to be reported.

CeO_2-encapsulated Pt nanostructures

Pt-based catalysts exhibit much higher catalytic activities and stabilities in many catalytic reactions. Most importantly, ultrafine Pt NPs with small particle sizes can be easily obtained as the seeds, which is beneficial for further enhancement of the catalytic activities and the coating process. Additionally, there is a strong synergistic effect between Pt and CeO_2, which could be attributed to the abundant oxygen vacancy defects, peerless oxygen storing/releasing capabilities and easy shuttling between the III–IV oxidation states of CeO_2. Consequently, CeO_2-encapsulated Pt nanostructures have been widely investigated.

Pt@CeO_2 core-shell hybrid nanostructures. Fabrication of the Pt@CeO_2 core–shell hybrid nanostructure is difficult because of the large lattice mismatch between Pt and CeO_2. To counterbalance the interfacial energy between Pt and CeO_2, embedding a layer of ligands and/or surfactant molecules between the core and sheath has been shown to be an effective method and is widely used.[74,75] The surface of the noble metal should be densely functionalized, and specific groups should be attached outside to promote the proximal growth of the metal oxide layer. In an example of successful surface modification of CeO_2, Xia's group used 6-aminohexanoic acid as a

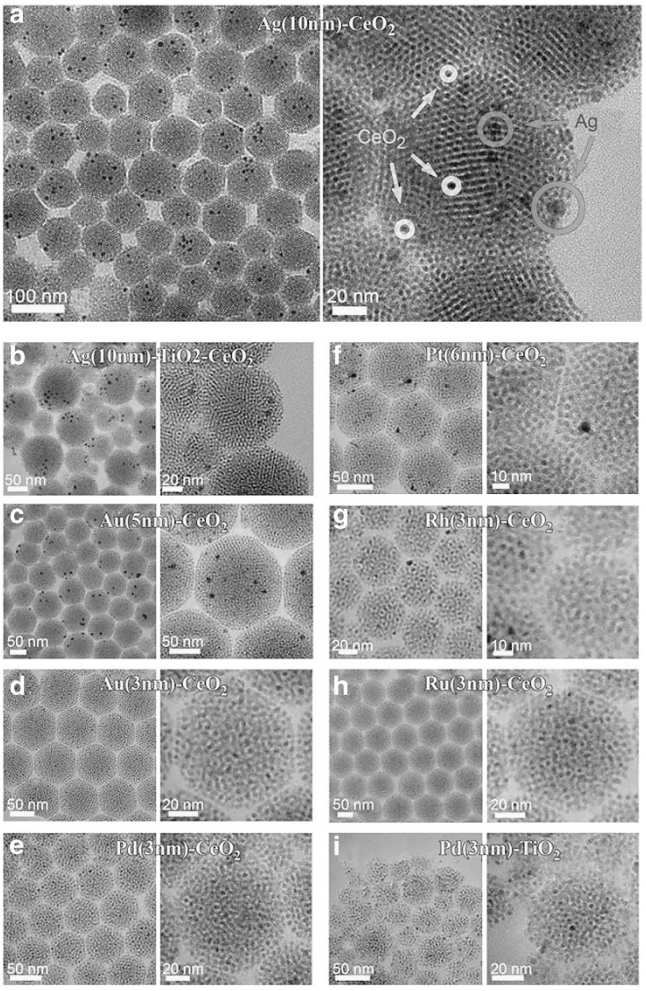

Figure 4 TEM images of mesoporous colloidal spheres built up by multiple components: (**a**) 10-nm Ag in porous CeO_2; (**b**) 10-nm Ag in porous TiO_2/CeO_2; (**c**) 5-nm Au in porous CeO_2; (**d**) 3-nm Au in porous CeO_2; (**e**) 3-nm Pd in porous CeO_2; (**f**) 6-nm Pt in CeO_2; (**g**) 3-nm Rh in porous CeO_2; (**h**) 3-nm Ru in porous CeO_2; and (**i**) 3-nm Pd in porous TiO_2. Reprinted with permission from Chen *et al.*[83] Copyright 2011 Wiley-VCH.

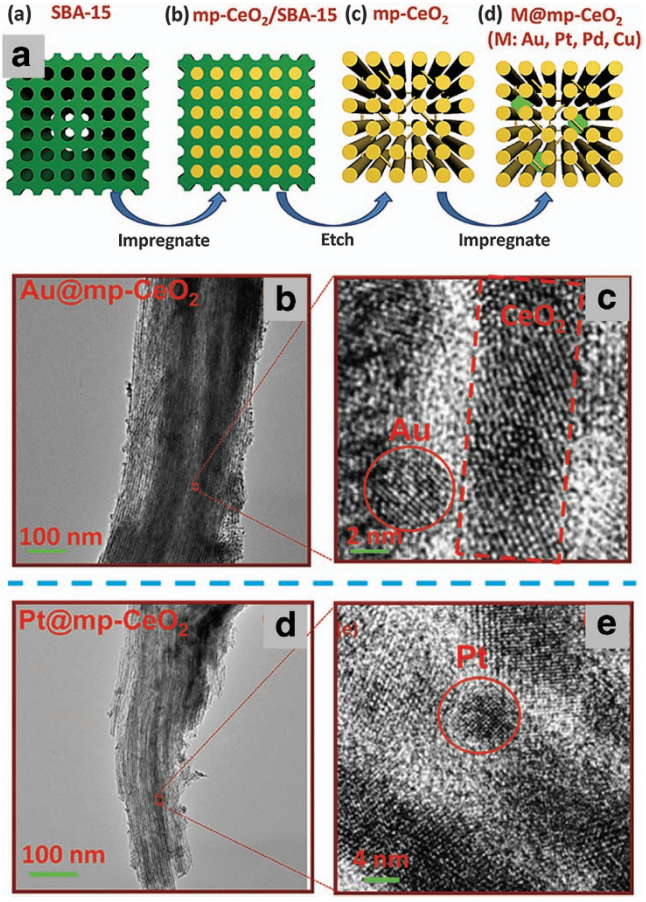

Figure 5 (**a**) Schematic representation of the synthesis of the noble metals@CeO_2 nanostructures; (**b**) large-scale image of Au@CeO_2; (**c**) HRTEM image of Au@CeO_2 showing the encapsulation of Au nanoclusters; (**d**) low-magnification TEM image of Pt@CeO_2; (**e**) HRTEM image showing the encapsulation of Pt nanoclusters. Reprinted with permission from Wen *et al.*[26] Copyright 2012 American Chemical Society.

capping molecule to limit the growth of CeO_2 and to maintain a positively charged particle surface such that the NPs can easily hybridize to Pt, which has a negative surface (Figure 1).[76] However, such a surface modification approach is yet to be successful in the fabrication of Pt@CeO_2 core–shell hybrid nanostructures.

Single core–shell Pt@CeO_2 nanospheres have also been successfully produced by Xu and coworkers via a heterogeneous seeded growth mechanism.[77] The seeded growth strategy is used to synthesize multicomponent core–shell hybrid nanostructures. Typically, this synthetic strategy can be divided into two separate steps: first, synthesis of uniform noble metal NPs with controllable morphologies, compositions and particle sizes, and second, by using the layer-by-layer coating technology to grow a dense layer of metal oxide on the core's surface. Uniform single core–shell Pt@CeO_2 hybrid nanostructures are obtained by using the data shown in Figure 2. Control of the growth rate of the shell component is the key factor that determines whether the synthesis will be successful. Notably, as reported in Xu's paper, the core–shell nanostructure can be finely tuned by simply changing the feeding amount of $CeCl_3$ added to an aqueous Pt colloid solution. Our understanding is that the hydrothermal approach and the usage of urea are very suitable for the formation of single core–shell nanostructures seeded by noble metals for the following reasons: (1) water is the most inexpensive, nontoxic and environment friendly solvent; (2) many inorganic salts have high solubility in water, which is very important for the homogeneous nucleation of shell components; and (3) such growth conditions could ensure that the rate of OH^- released is slow enough to efficiently avoid the independent nucleation of the shell component.[74]

In addition to the single core–shell sample, preparation of the Pt@CeO_2 multi-core–shell hybrid nanostructure has been reported via one-pot methods that are driven by special forces. Our previous report[78] noted that Ce^{3+} exhibits greater reducing capability in alkaline conditions than in neutral ones. A redox reaction can be easily triggered on the two-face interface between Pt metal salt with high oxidation potential and $Ce(OH)_3$ precursor. Uniform and monodisperse sphere-like Pt@CeO_2 multi-core–shell hybrid nanostructures are prepared on a large scale. The transmission electron microscopic (TEM) images are shown in Figure 3; in each sphere-like nanostructure, thousands of small CeO_2 NPs (6.2 nm in average) assembled to form a dense shell outside. Because their deeper contrast compared with CeO_2, the Pt NPs beneath the shell can be clearly distinguished. It is believed that the formation process of such superstructures involves two separate steps: first, the nucleation and growth of Pt and CeO_2

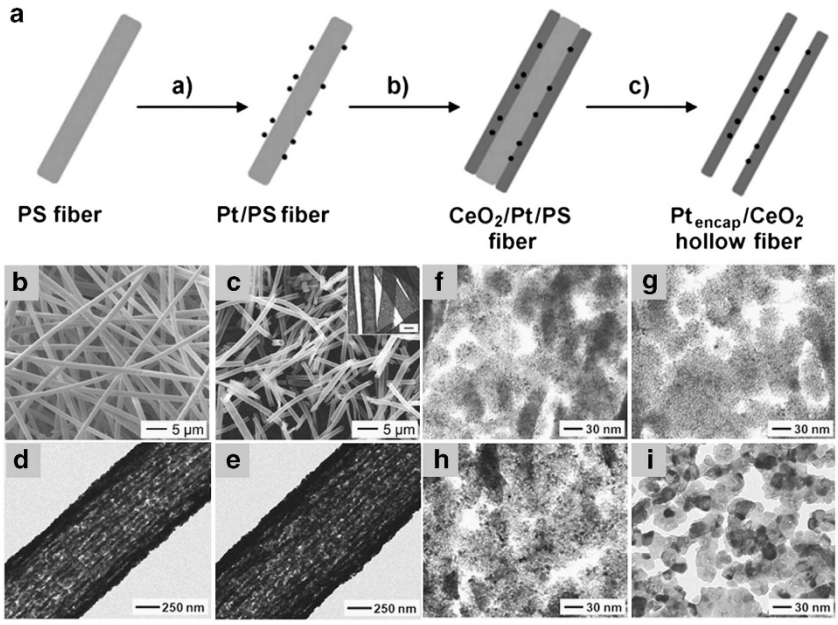

Figure 6 (**a**) Schematic representation of the synthesis of the Pt–CeO_2 hollow fiber nanostructures; (**b** and **c**) SEM images of PS/Pt/CeO_2 core–shell fibers (**b**) before and (**c**) after calcination; (**d** and **e**) low-magnification TEM images of Pt/CeO_2 hollow fibers after calcinations at 400 °C (**d**) and 800 °C (**e**) for two hours in air; (**f**–**i**) high-magnification TEM images of Pt/CeO_2 hollow fibers after calcinations at 400 °C (**f**), 500 °C (**g**), 600 °C (**h**) and 800 °C (**i**). Reprinted with permission from Yoon *et al.*[85] Copyright 2012 Wiley-VCH.

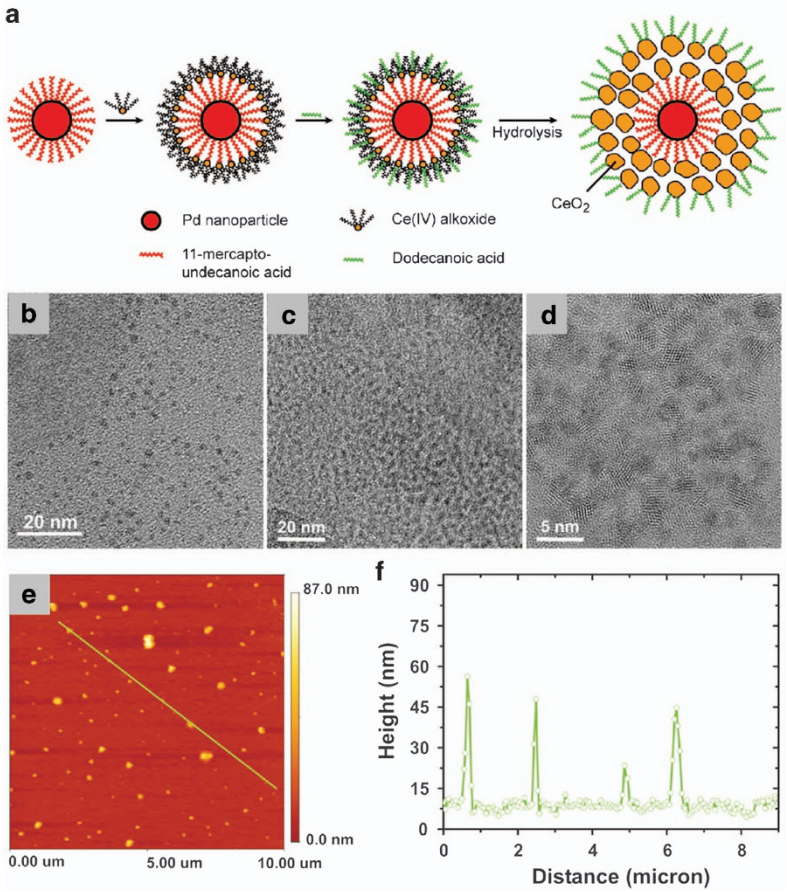

Figure 7 (**a**) Schematic representation of the synthesis of the Pd@CeO_2 core-shell nanostructure; (**b**) TEM image of MUA-protected Pd NPs; (**c** and **d**) HRTEM images of Pd@CeO_2 core–shell NPs; (**e** and **f**) AFM image and line-height measurement of Pd@CeO2 NPs. Reprinted with permission from Cargnello *et al.*[87] Copyright 2012 American Chemical Society.

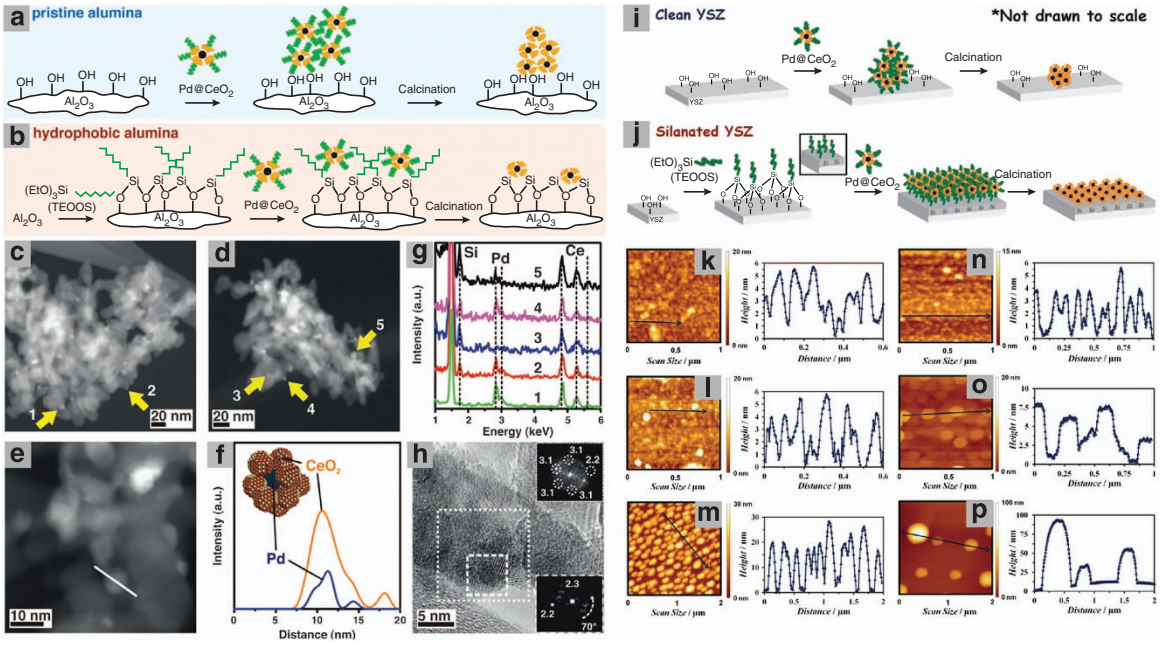

Figure 8 Schematic representation of the agglomeration of Pd@CeO_2 structures by using pristine alumina (**a**) and their deposition as single units after treatment of the same support with triethoxy(octyl)silane (TEOOS) (**b**); HAADF-STEM images of Pd@CeO_2 core–shell nanostructures dispersed on hydrophobic Al_2O_3 after calcining at 500 °C (**c**) and 850 °C for 5 h (**d**); EDS spot analysis (**g**); high-magnification HAADF-STEM images of Pd@CeO_2/Al_2O_3 products after being calcined at 500 °C (**e**); the corresponding EDS line profile (**f**); HRTEM image of a single Pd@CeO_2 structure on the Pd@CeO_2/H-Al_2O_3 catalysts calcined at 500 °C (**h**). Reprinted with permission from Cargnello *et al.*[86] Copyright 2012 Science. Overview of the deposition of Pd@CeO_2 nanostructures on (**i**) clean YSZ (100) and (**j**) alkyl-siloxane functionalized YSZ (100); AFM topography images with representative line scans for Pd@CeO_2 deposited on alkyl-siloxane functionalized YSZ (100) after calcination in air at 723 K (**k**), 973 K (**l**), 1373 K (**m**); and Pd@CeO_2 deposited on clean YSZ (100) after calcination in air at 723 K (**n**), 973 K (**o**), 1373 K (**p**). Reprinted with permission from Adijanto *et al.*[90] Copyright 2013 American Chemical Society.

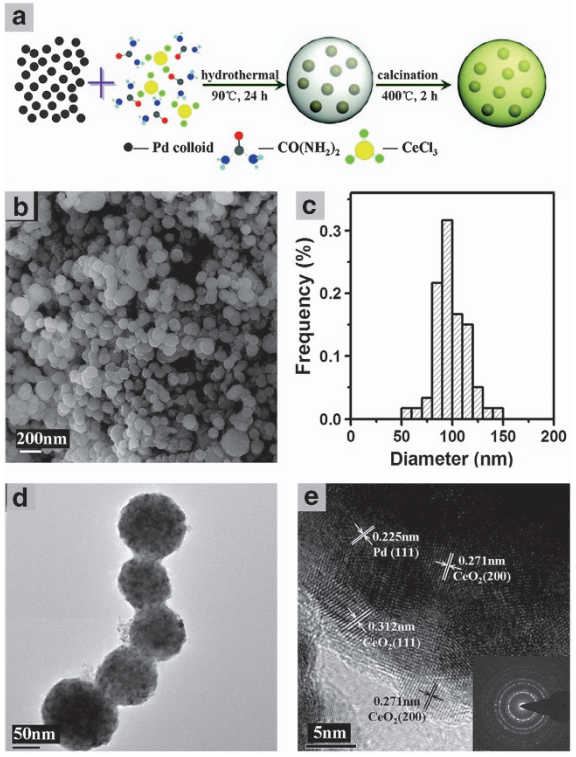

Figure 9 (**a**) Schematic representation of the synthesis of the Pd@CeO_2 nanospheres; (**b**) SEM image of Pd@CeO_2 nanospheres; (**c**) particle-size distribution of Pd@CeO_2; (**d** and **e**) TEM and HRTEM images of Pd@CeO_2. Reprinted with permission from Zhang *et al.*[91] Copyright 2011 American Chemical Society.

NPs, followed by the self-assembly of the two components. In the nucleation – growth stage, the zeta potential of the $Ce(OH)_3$ surface has been reported to be +25.9 mV. The positive surface has a strong attractive force for the negative $PtCl_4^{2-}$ anions. These anions could be strongly attracted to the $Ce(OH)_3$ surface via electrostatic interactions. Then, an auto-redox reaction occurs on the surface of the CeO_2 NPs. When the ultra-small Pt NPs are formed, the $Ce(OH)_3$ precursors are oxidized to CeO_2 at the same time. Thus, the original strongly coupled Pt–CeO_2 self-assembled hybrid structures are formed.

Embedded Pt NPs in porous CeO_2 nanostructures. Another efficient way to encapsulate Pt NPs in CeO_2 is to embed them into a porous nanostructure. Stucky's group has published a series of reports of the successful fabrication of mesostructured silica or other metal oxides.[79–82] The pores provide enough space for noble metal growth; however, the limited space of the channel can limit the overgrowth of noble metals, and the hard framework of CeO_2 can separate the Pt NPs far away from one another even during long-term high-temperature treatment or catalytic application. The porous CeO_2 can be either a single crystal or a closely packed 3D structure composed of tiny CeO_2 NPs. A representative protocol was reported by Li and coworkers.[83] They used the van der Waals' force as the driving force to trigger the self-assembly of oleic acid-modified noble metals and CeO_2 NPs to form a multicomponent porous structure (Figure 4). For both the hard template and wet chemistry methods, the aims are the same: to stop the mass transformation process of the unstable noble metals by fixing them in CeO_2 cages.

Mesostructured metal oxides are among the most important types of catalysts and have attracted great interest because of their ultra-large specific surface area and uniform channel interconnectivity for gas

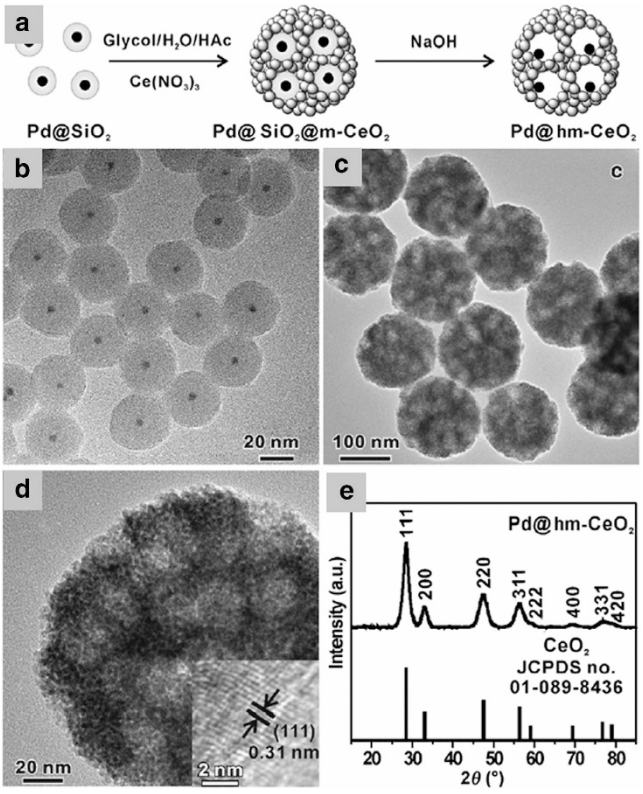

Figure 10 (**a**) Schematic representation of the synthesis of the Pd@CeO_2 multi-yolk-shell nanostructures; (**b**) TEM image of Pd@SiO_2; (**c**) TEM image of Pd@CeO_2; (**d**) HRTEM image of Pd@CeO_2; (**e**) XRD data of Pd@CeO_2 nanostructures. Reprinted with permission from Chen *et al.*[92] Copyright 2012 Wiley-VCH.

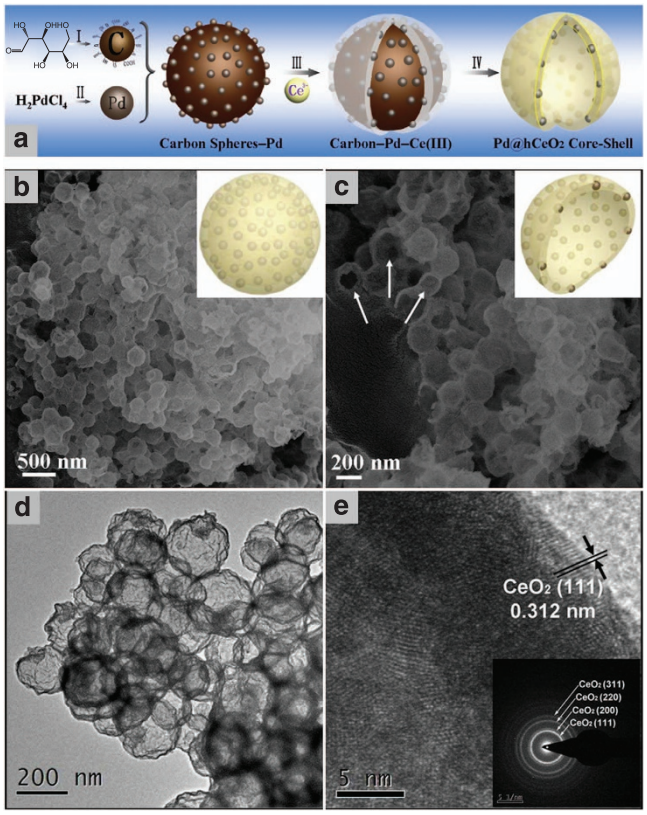

Figure 11 (**a**) Schematic representation of the synthesis of the Pd@CeO_2 core-shell hollow nanospheres; (**b** and **c**) SEM images of the as-prepared Pd@CeO_2; (**d**) TEM image of Pd@CeO_2; and (**e**) HRTEM image of Pd@CeO_2. Reprinted with permission from Zhang *et al.*[93] Copyright 2013 American Chemical Society.

diffusion and host–guest interactions. Various techniques, including conventional sol-gel synthesis procedures, template growth, chemical vapor deposition and spray pyrolysis, have been developed for the synthesis of mesoporous metal oxides for new applications. Corma and coworkers used the block copolymer ($EO_{20}PO_{70}EO_{20}$, Pluronic P123) as a template to produce mesostructured CeO_2 and CeO_2–SiO_2 materials with high thermal stability.[84] The assembly process is controlled by adjusting the interactions of a copolymer template with the CeO_2 NPs and SiO_2. Subsequently, 2–3-nm Pt nanocrystals are embedded within ultrathin layers of highly structured SiO_2 binder via wet impregnation of the CeO_2–SiO_2 support and CeO_2 support in a Pt salt solution. Catalysis of the chemoselective hydrogenation of an α, β-unsaturated aldehyde such as crotonaldehyde is performed, and the resulting catalyst is satisfactorily active and selective. Recently, Tao and coworkers encapsulated Pt and other noble metals in channels of mesoporous CeO_2, in which SBA-15 silica is used as a hard template to synthesize mesoporous CeO_2, and metal nanoclusters are formed on the internal surface of the wall of channels via a conventional impregnation method (Figure 5).[26]

Encapsulated Pt NPs in the inner walls of hollow CeO_2 nanostructures. Loading the Pt NPs on the surfaces or the inner walls of CeO_2 could yield vastly different stabilities. Simply loading the Pt NPs makes it difficult to prevent their secondary growth because of strong Brownian motion. If a collision occurred between different CeO_2 NPs, the surface-loaded Pt NPs have a better chance to further their growth, but such a situation could not occur for the Pt NPs encapsulated by the inner walls of the hollow CeO_2 nanostructure. Xia and coworkers reported a hard template method for embedding Pt NPs in the inner surfaces of CeO_2 hollow fibers with open ends to generate a new catalytic system.[85] As shown in Figure 6a, polystyrene fibers are first used as the hard template to guide the growth of the 1D nanostructure. After the selective deposition of Pt NPs on the surface of the polystyrene fibers, a dense CeO_2 layer is placed outside and sintered at high temperature such that the small Pt NPs have been strongly encapsulated by the inner walls of the hollow CeO_2 fibers. The as-prepared Pt/CeO_2 nanostructures exhibit satisfactory thermal stability against sintering of as high as 700 °C and catalytic activity with CO oxidation (2–3 orders of magnitude higher than those of other systems).

CeO_2-encapsulated Pd nanostructures

The growth in demand and the ultrahigh price level have seriously limited a broader application of Pt nanocatalysts. Therefore, the development of 'Pt-free' CeO_2-based noble metal catalysts has generated much interest in recent years. Compared with Au and Ag, Pd has the closest catalytic performance to Pt in many catalytic reactions. In fact, for several such reactions, the Pd catalyst exhibits higher activity than Pt. For example, in organic chemistry, numerous carbon–carbon bond forming reactions, such as Suzuki, Heck and Stille couplings, depend on catalysts based on Pd or its compounds. Moreover, supported PdO_x is recognized as one of the best catalysts for catalytic CH_4 combustion. Unfortunately, Pd has poor stability; it is difficult for Pd to maintain its size and shape under

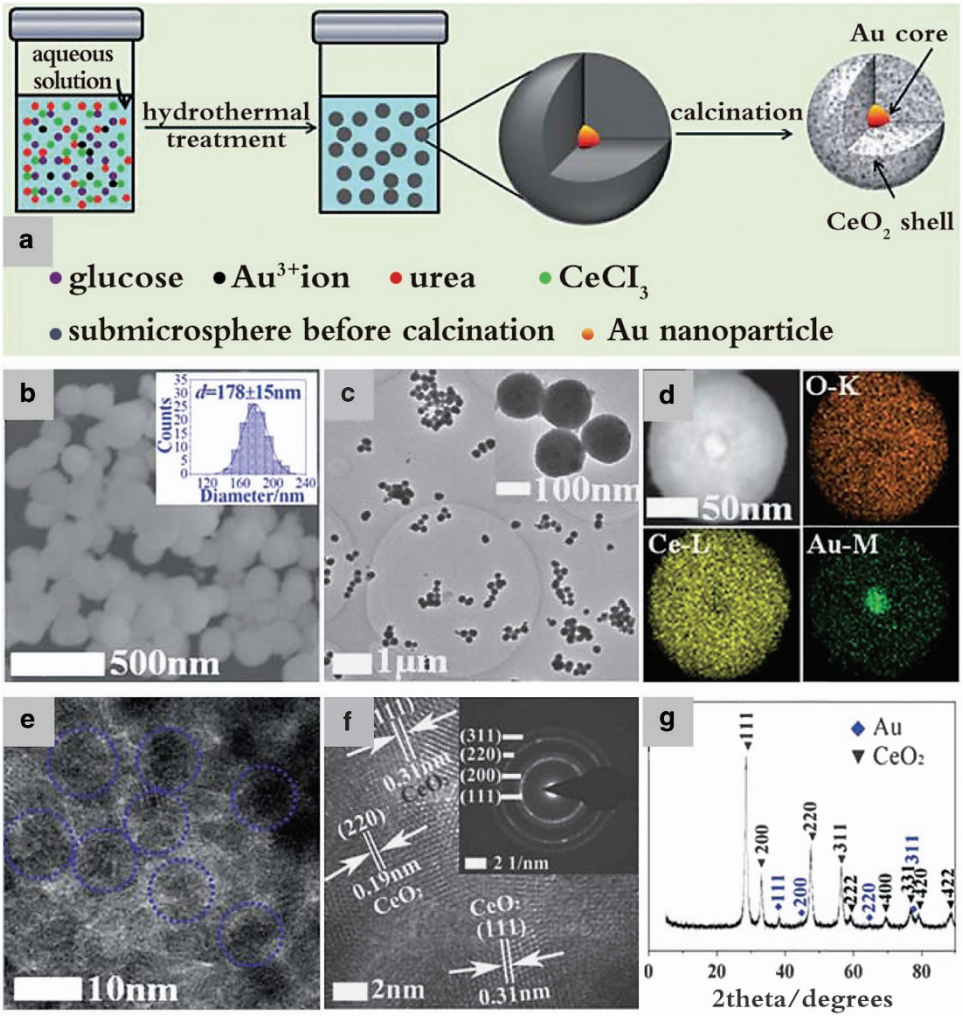

Figure 12 (**a**) Schematic representation of the synthesis of the Au@CeO_2 core-shell nanostructures; (**b**) SEM images and (**c**) TEM images of the as-obtained Au@CeO_2; (**d**) Mapping analysis of Pd@CeO_2; (**e** and **f**) HRTEM images of Au@CeO_2; (**g**) XRD data of Au@CeO_2. Reprinted with permission from Qi *et al.*[94] Copyright 2013 Royal Society of Chemistry.

high-temperature conditions. Thus, the formation of CeO_2 encapsulated by Pd nanostructures is required for actual industrial processes.

Pd@CeO_2 core-shell hybrid nanostructures. The core–shell hybrid nanostructure is another important Pd/CeO_2 hybrid structure. A typical Pd@CeO_2 core–shell nanostructure was constructed by Gorte and coworkers via a supramolecular self-assembly process.[86] The synthesized procedure consists of the following three steps: (1) the use of difunctional 11-mercaptoundecanoic acid as the capping molecular to protect ultra-small Pd NPs; (2) a self-assembly process triggered by adding a Ce precursor (cerium(IV) tetrakis(decyloxide)) to the solution; and (3) controlled hydrolysis to obtain dispersible Pd@CeO_2 nanostructures. The corresponding TEM and atomic force microscopic images clearly demonstrated the effectiveness of these three steps (Figures 7b–e).

The as-produced core–shell sample is functionalized with dodecanoic acid, and the hydrophobic alkyl surface state is repelled by the hydrophilic surface of most oxide supports, such as Al_2O_3 and yttria-stabilized zirconia (YSZ). As a result, when they are dropped onto planar supports, the hydrophilic Pd@CeO_2 NPs have a strong tendency to aggregate, which makes them unsuitable for their catalytic applications. Gorte and coworkers conducted a further surface modification process on the second supporters to make the hydrophobic functional groups remain on their surface such that the Pd@CeO_2 sample can be uniformly dispersed on the substrate's surface. As shown in Figures 8c–f and K to P, a series of supported Pd@CeO_2 catalysts have been successfully fabricated, including Pd@CeO_2/Al_2O_3[87–89] and Pd@CeO_2/YSZ,[90] owing to the presence of a strong interaction driven by Van der Waals forces between the Pd@CeO_2 sample and modified Al_2O_3 or YSZ. Additional atomic force microscopic images have further confirmed the uniformity of the Pd@CeO_2 samples.

In addition to this supramolecular chemistry strategy, seeded growth methods have been successful in the synthesis of the Pd@CeO_2 core–shell nanostructure. Xu's group reported a facile, low-temperature hydrothermal synthesis of 'plum pudding'-structured Pd@CeO_2, which is similar to the previously reported Pt@CeO_2 (Figure 9).[90] In their work, polyvinylpyrrolidone-stabilized Pd NPs are used as seeds, and the CeO_2 coating process is finished via a hydrothermal treatment.

Pd@CeO_2 yolk–shell hybrid nanostructures. In contrast to core–shell structures, which have solid cores, yolk–shell structures have a mobile core inside and fixed sheath outside, which gives such hybrid

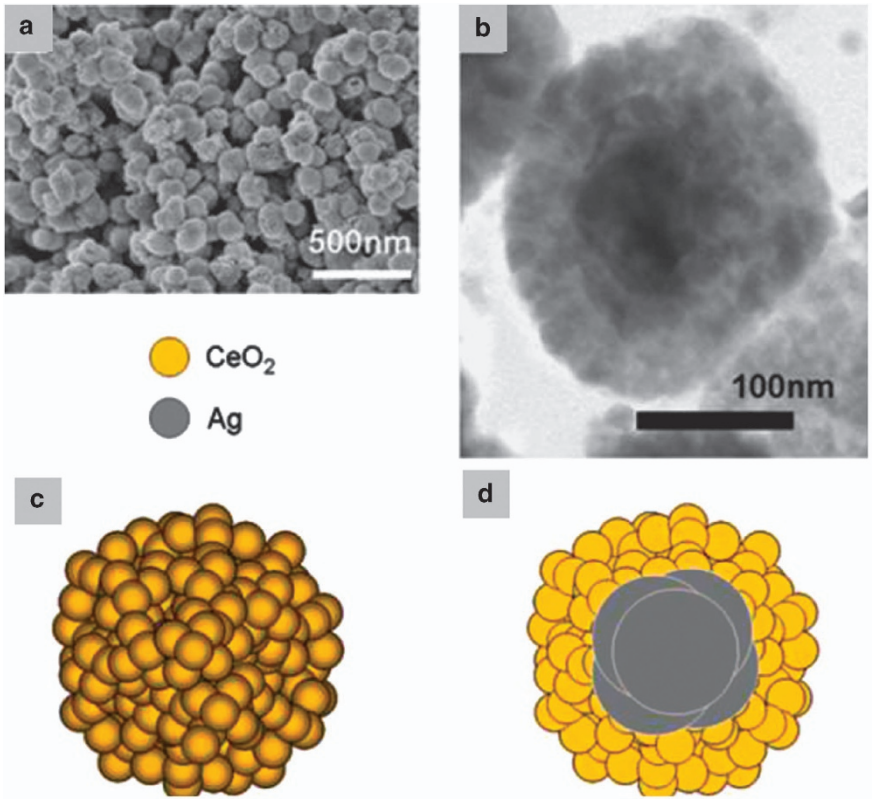

Figure 13 (**a**) Low-magnification SEM image of Ag@CeO_2 and (**b**) high-magnification TEM image of single Ag@CeO_2 nanospheres; (**c** and **d**) schematic illustrations of Ag@CeO_2. Reprinted with permission from Kayama *et al.*[95] Copyright 2010 American Chemical Society.

structures special properties, including low density, high surface area and interstitial hollow spaces. The void between the core and shell is very important because the space ensures that the active cores are infiltrated in the reaction solution, which is helpful in enhancing catalytic performance in a liquid-phase catalytic reaction. Typically, one of three synthetic strategies is used to produce a yolk–shell nanostructure. (1) The hard-templating method, the most common strategy, in which the presynthesis of noble metal cores is followed by further coating them with a transitional layer (for example, SiO_2, C or polymer). The template for this layer should be easy to remove after the synthesis, and the target shell materials are deposited onto the surface of the template to form a sandwiched nanostructure, followed by the selective removal of the template layer by using dissolution with a solvent or calcination with heating. (2) The soft-templating method, in which the synthetic mechanism is similar to that of the hard-templating method, with the only significant difference being that it uses the organic long-chain molecules to occupy the space between the core and shell instead of a crystal layer. (3) The template-free method, in which, for some conditions, the original core–shell structure can be translated into a yolk–shell structure, which is driven by the Ostwald ripening force.

Zheng and coworkers successfully synthesized multi-yolk–shell Pd@CeO_2 nanocatalysts via the hard-templating method, by using the data shown in Figure 10.[91] First, uniform and monodisperse Pd-Fe_2O_3@SiO_2 core–shell nanospheres are prepared in a reverse micelle system with the help of Brij 56 molecules. After acid has been used to etch the part of Fe_2O_3, $Ce(NO_3)_3$ is added in a mixture of water, ethylene glycol, acetic acid and the as-obtained Pd@SiO_2 core–shell sample in a solvothermal process to form a Pd@SiO_2@CeO_2 multi-sheath superstructure. Further selective removal of silica with a NaOH solution causes the multi-core–shell sample to transform into a multi-yolk–shell nanostructure.

Encapsulated Pd NPs in the inner walls of hollow CeO_2 nanospheres. Hollow structures have attracted great interest because of their promising applications in various areas, including catalysis, drug delivery, gas sensors, energy conversion and storage systems. Xu's group developed a new method for fixing the unstable Pd NPs into a hollow CeO_2 nanostructure (Figure 11).[92] They use carbon nanospheres as the hard templates to deposit 1–5-nm Pd NPs on the surface. Subsequently, a dense layer of CeO_2 is coated on the Pd/C hybrid nanospheres. Finally, the inside carbon nanospheres can be easily removed via a simple heating process. Unlike the multi-yolk–shell sample, the Pd is immobile, but there is still a large space inside the nanospheres. The core–shell strategy efficiently prevents the aggregation of Pd NPs during the high-temperature calcination process and the leaching of Pd NPs for the catalytic reaction in a liquid phase.

CeO_2-encapsulated Au and Ag nanostructures

The catalytic activities of Au and Ag NPs should not be overlooked. These materials also have an important role in certain applications. Although Au/SiO_2, Au/ZrO_2, Au/ZnO and Au/TiO_2 have been widely synthesized and studied in depth, very little such research has been conducted on Au/CeO_2 and Ag/CeO_2.

Au@CeO_2 and Ag@CeO_2 core–shell hybrid nanostructures. As a typical example, Tang and coworkers have described a 'self-templating' technique to synthesize uniform Au@CeO_2 core–shell submicrospheres.[93] In the initial reaction, $HAuCl_4$, $CeCl_3$, glucose and

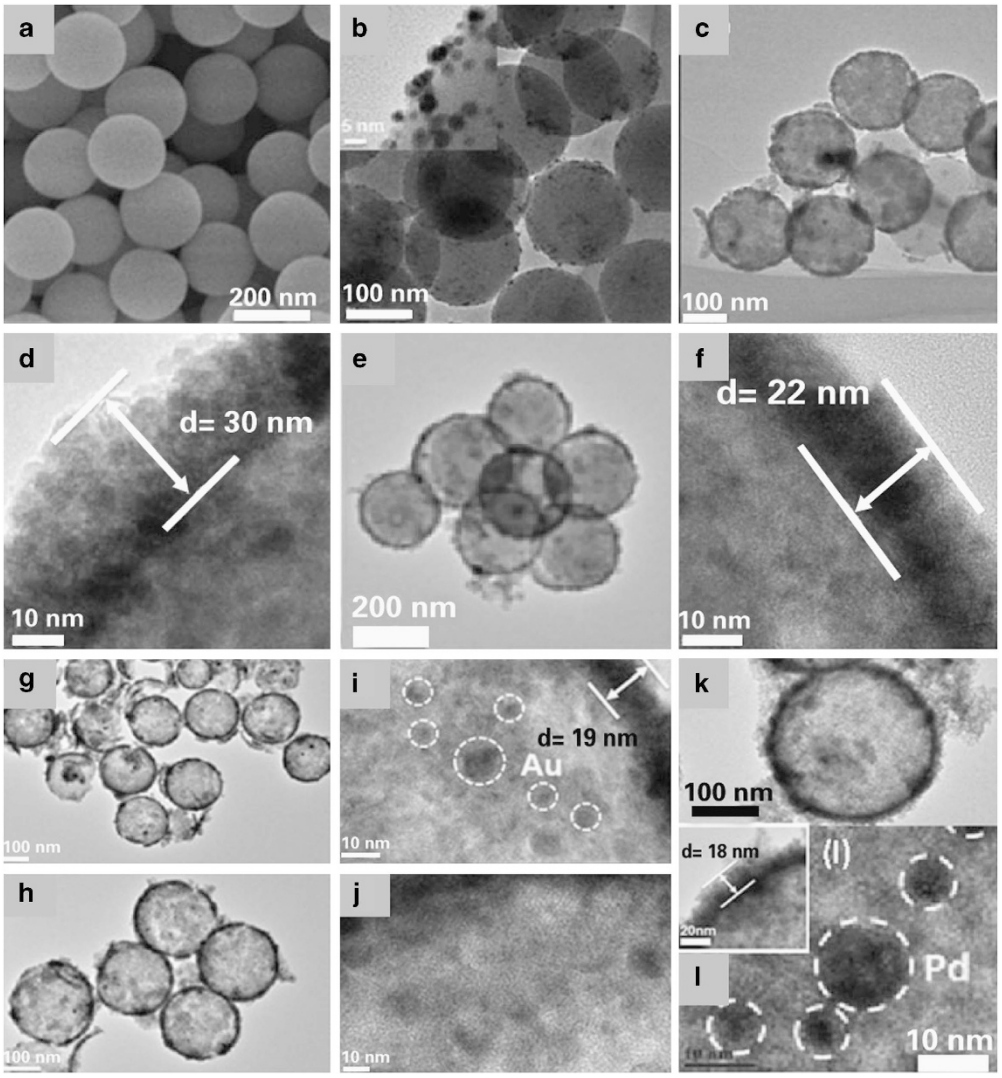

Figure 14 (**a**) SEM image of SiO_2 and TEM images of (**b**) Au/SiO_2; (**c** and **d**) SiO_2/Au@CeO_2; (**e** and **f**) SiO_2/Pd@CeO_2; (**g**–**j**) @Au/CeO_2; and (**k**,**l**) @Pd/CeO_2 nanospheres. Reprinted with permission from Liu *et al.*[98] Copyright 2013 Royal Society of Chemistry.

urea are mixed in water, followed by a hydrothermal treatment to produce a sphere-like precursor. As shown in Figure 12, the magnified TEM images confirmed that the submicrospheres have a core–shell nanostructure with sub-17-nm Au NPs inside. Analysis of the TEM results indicates that two separate steps occur during this hydrothermal process. First, the redox reaction between $HAuCl_4$ and glucose is induced by increasing the reaction temperature. Then, the condensation of glucose in solution under hydrothermal conditions leads to the formation of amorphous carbon submicrospheres with Au as cores inside, and the adsorption of Ce ions simultaneously occurs with the growth of the carbon matrix. To transfer the noncrystal Ce/C mixture into the CeO_2 crystal, the as-obtained precursors are calcined in air. The corresponding TEM, scanning transmission electron microscopic and mapping images reveal that the final products maintain their core–shell structure, and the X-ray diffraction spectra indicate that both the Au and CeO_2 structures maintained high crystallinities.

Ag has the poorest stability of the noble metals. Because of the high Ksp (solubility product) values of the types of Ag-based compounds, such as AgCl, AgBr, AgI, $Ag(NH_3)_2^+$ and Ag_2S, Ag NPs can be etched by many types of ions, including Cl^-, Br^-, I-, S^{2-}, NH_3 and O^{2-}. As a result, it is very difficult to synthesize CeO_2-encapsulated Ag nanostructures via the seeded growth method. The most successful work has been reported by Kayamaand coworkers (Figure 13). They established a new mechanism, 'autocatalyzed redox reaction,' to synthesize riceball-like Ag@CeO_2 core–shell nanostructures.[94–96] Typically, a mixed aqueous solution of $Ce(NO_3)_3$ and $AgNO_3$ is added to stirred aqueous ammonia, causing an auto-redox reaction and yielding a precipitate. There are four steps involved in this reaction: (1) the nucleation of $Ce(OH)_3$ and Ag(OH); (2) the dissolution of Ag(OH) and formation of $[Ag(NH_4)_2]^+$ driven by thermodynamics (Ksp($[Ag(NH_4)_2]^+$) ≫ Ksp(Ag(OH))); (3) the auto-redox reaction between $Ce(OH)_3$ and $[Ag(NH_4)_2]^+$ on the surface of crystallized $Ce(OH)_3$; and (4) an additional self-assembled process to form the final Ag@CeO_2 riceball-like core–shell hybrid NPs. This facile one-pot aqueous methodenables large-scale synthesis.

Encapsulated Au NPs on the inner walls of hollow CeO_2 nanospheres. Figure 14 shows the TEM images of encapsulated Au NPs on the inner

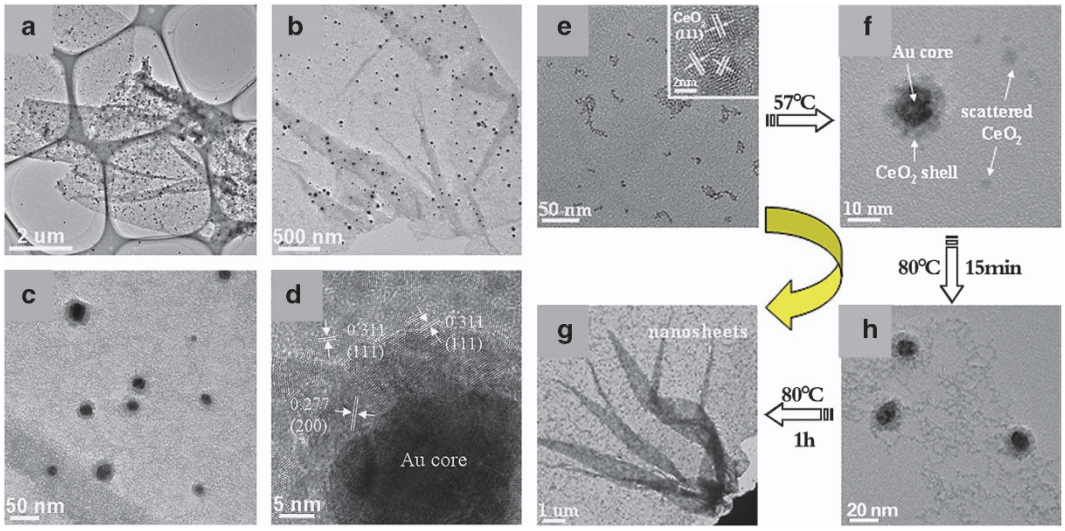

Figure 15 (**a**–**c**) Low-magnification TEM images of Au–CeO_2 hybrid nanosheets; (**d**) high-magnification TEM image of Au-CeO_2 hybrid nanosheet; (**e**–**h**) structural evolution, TEM images acquired at different reaction times: (**e**) after addition of butylamine; (**f**) after the solution was heated to 57 °C; (**g**) after the solution reached 80 °C and was kept there for 15 min; and (**h**) after the solution was is maintained at 80 °C for 1 h. Reprinted with permission from Wang *et al.*[99] Copyright 2012 Royal Society of Chemistry.

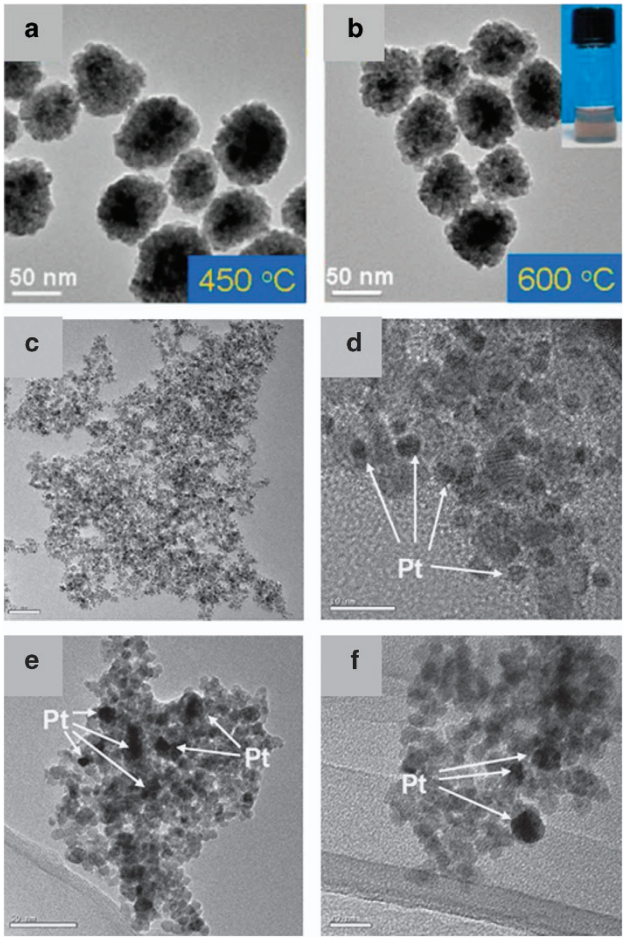

Figure 16 Low-magnification TEM images of Pt@CeO_2 multi-core-shell nanospheres after calcinations at 450 °C (**a**) and 600 °C (**b**) for 5 h; (**c** and **d**) TEM images of directly mixed Pt–CeO_2 sample; (**e** and **f**) TEM images of directly mixed Pt–CeO_2 sample after calcinations at 600 °C for 5 h. Reprinted with permission from Wang *et al.*[78] Copyright 2013 American Chemical Society.

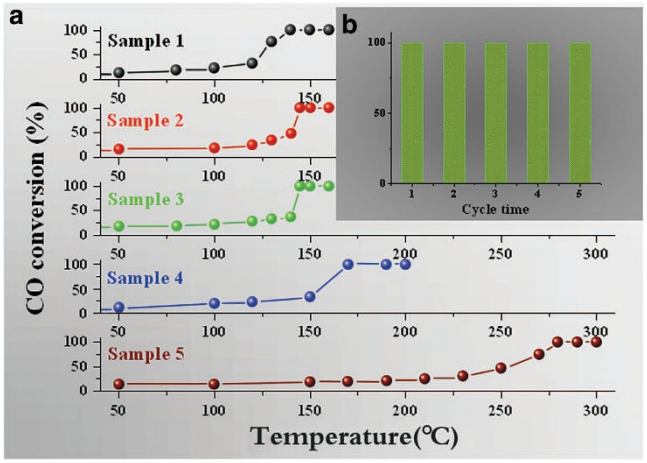

Figure 17 (**a**) CO conversion curves of Pt@CeO_2 and Pt–CeO_2 sample; (**b**) cycling test (150 °C) of Pt@CeO_2 sample after calcinations at 600 °C for 5 h. Every 8 mg of catalysts is mixed with 20 mg of SiO_2 (the SiO_2 powder was purchased from Aladdin Company (Shanghai, China) with a particle size of 15 nm ± 5 nm). Reprinted with permission from Wang *et al.*[78] Copyright 2013 American Chemical Society.

walls of hollow CeO_2 nanospheres, which were reported by Zhang and coworkers.[97] The 'hard-templating' method used is similar to that for the aforementioned Pt@CeO_2 hollow nanofiber and Pd@CeO_2 hollow nanospheres. The difference is that Zhang's group used a SiO_2 layer as the hard template. Compared with other carbon materials, such as carbon nanofibers and amorphous carbon nanospheres, SiO_2 has two unparalleled advantages. First, the Stöber sol-gel method is very mature. Uniform SiO_2 spheres with different particle sizes can be synthesized very simply on a large scale. Second, the removal of SiO_2 is straightforward in alkali solutions at room temperature; it is unnecessary to use a high-temperature calcination process. However, an obvious disadvantage remains: compared with a carbon template, a SiO_2 template requires surface modifications to allow further hybridization with noble metals. In the authors' study, 3-amino

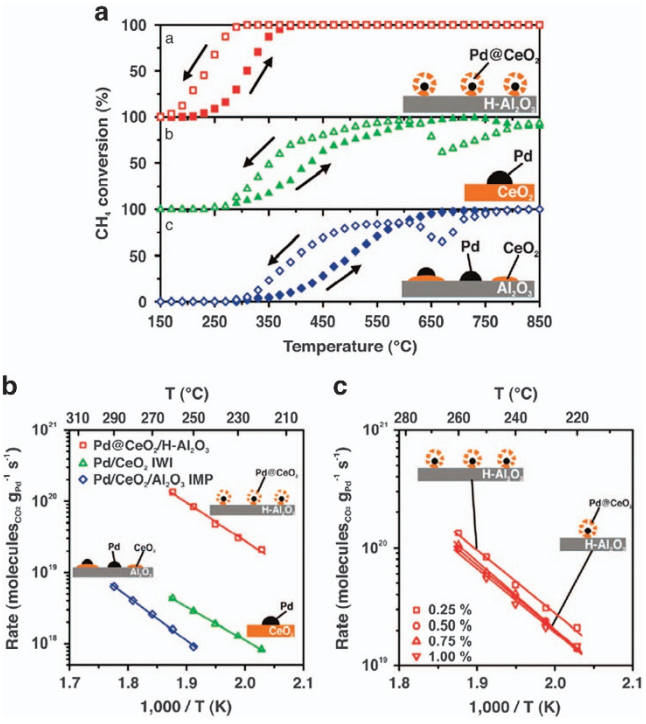

Figure 18 (**a**) Heating and cooling (10 °C min–1) light-off curves of CH_4 conversion as a function of temperature for the three catalyst formulations used. Kinetic rate data for CH_4 oxidation on (**b**) $Pd@CeO_2/Al_2O$ core-shell catalyst, Pd/CeO_2, and $Pd/CeO_2/Al_2O_3$. (**c**) $Pd@CeO_2/Al_2O_3$ core–shell catalysts at different loadings of the structures (the Pd/Ce weight ratio is maintained at 1/9): Pd loading of 0.25, 0.50, 0.75 and 1.00%. Reprinted with permission from Cargnello *et al.*[86] Copyright 2012 Science.

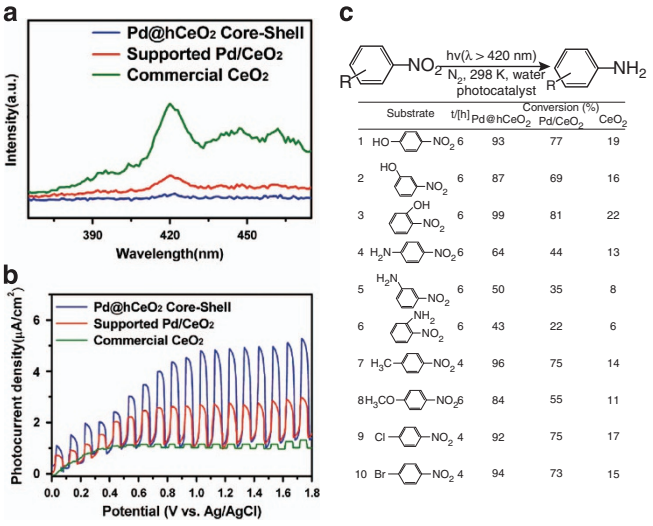

Figure 19 (**a**) Photoluminescence spectra of commercial CeO_2, supported Pd/CeO_2, and $Pd@CeO_2$ core–shell sample; (**b**) chopping visible-light photocurrent – voltage curves of commercial CeO_2, supported Pd/CeO_2 and $Pd@hCeO_2$ core-shell nanocomposites in 0.2 M Na_2SO_4 (pH 6.8) aqueous solution versus Ag/AgCl; (**c**) photocatalytic reduction of substituted aromatic nitro compounds over $Pd@hCeO_2$ core–shell nanocomposite, supported Pd/CeO_2 and commercial CeO_2 aqueous suspension under visible-light irradiation ($\lambda > 420$ nm) with the addition of ammonium oxalate as a quencher for photogenerated holes and N_2 purge at room temperature. Reprinted with permission from Zhang *et al.*[93] Copyright 2013 American Chemical Society.

propyl-3-methyl silane was used to modify the SiO_2 surface to embed a mass of amino groups on the surfaces, which favors the anchoring of noble metal NPs.

Encapsulated Au NPs into CeO_2 nanosheets. Our group has also focused on a Au–CeO_2 hybrid system.[98] We observed that a one-pot self-assembly synthesis could be induced by the addition of $HAuCl_4$, $Ce(NO_3)_3$, L-lysine, polyvinylpyrrolidone and butylmine in water at 80 °C for 1 h. Figure 15 shows the corresponding TEM images of the as-obtained Au–CeO_2 hybrids with graphene-like nanostructures. Many drapes were observed in the final products, which could be attributed to the self-folding behavior of the 2D nanostructure. In Figure 15c, uniform Au NPs with an average diameter of 20 nm can clearly be seen because of their greater contrast compared with CeO_2 NPs, and the high-resolution TEM image in Figure 15d distinctly shows the components of both the core and shell. To determine the growth mechanism of such a unique hybrid nanostructure, the TEM images acquired at different reaction times were tested carefully. As shown in Figures 15e–h, after butylamine was added to the solution, only 4-nm CeO_2 NPs exhibited no Au NPs. The reaction solution appeared dark green when the temperature reached 57 °C. The corresponding TEM image in Figure 15f confirms that the Au NPs grew to as much as 20 nm and that the original core–shell nanostructure was formed. The solution turned purple after the temperature reached 80 °C. Finally, the self-assembled sheet-like nanostructure is shown in Figure 15g, which indicates that the L-lysine molecules increased the reduction potential of Au^{3+}, and, after the formation of the Au^{3+}–L-lysine complex, Au^{3+} could be reduced only at a temperature higher than 57 °C.

CATALYTIC APPLICATIONS

The interface between the noble metal and CeO_2 has been considered an excellent site for many catalytic reactions. For example, CeO_2-based noble metal hybrid catalysts have great efficacy with the CO oxidation reaction, water–gas shift reaction, methanol steam reforming reaction, carbon oxidation reaction, methane combustion reaction, selective oxidation and reduction reaction in the organic liquid phase, and even with some electrochemical catalytic reactions. The hybrid nanostructure has a considerable effect on its catalytic performance. Compared with the traditional catalysts with surface loading, the CeO_2-encapsulated noble metal catalysts exhibited much higher activity, stability and selectivity. The reasons for their superior properties are as follows: (1) the encapsulated nanostructure can provide an excellent opportunity for controlling the interaction among different components; (2) the core–shell and yolk–shell nanostructures can maximize the interface area, and the noble metal centers are closely surrounded by metal oxide supports, which is very beneficial in providing more active centers and novel synergistic effects to increase the reaction speed; and (3) the noble metals are fixed strongly within the CeO_2 nanostructures, in which the individual noble metal NP is isolated and separated by a layer of metal oxide supports, which can efficiently stop the mass transformation process during the thermal treatment or catalytic process.

Anti-sintering capabilities

Anti-sintering capability is required for applications. For example, three-way catalysts should work above 400 °C, and in the methane combustion reaction, the high stability of methane hinders the catalytic reaction; hence, the complete conversion temperature is

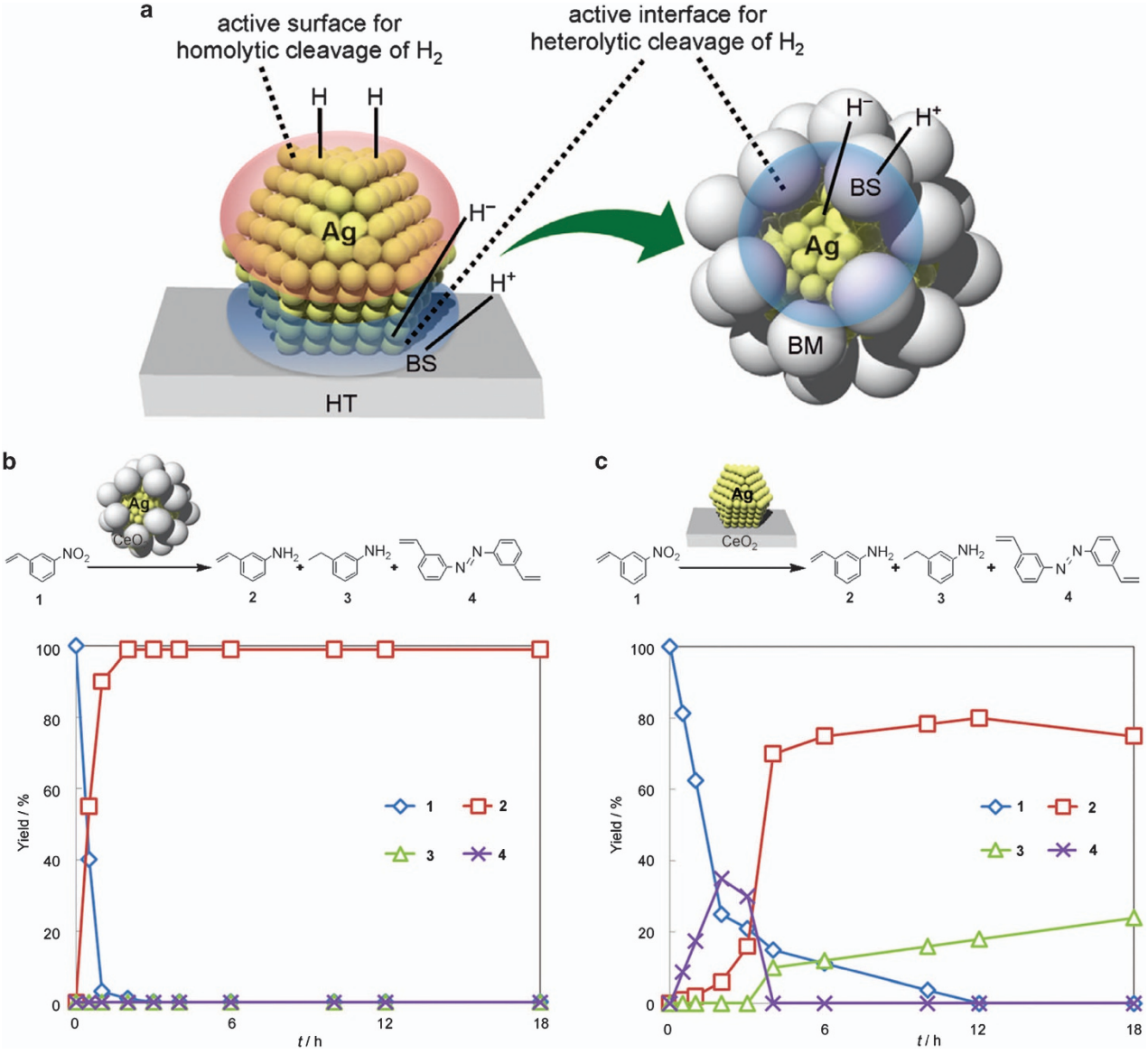

Figure 20 (**a**) Catalyst design of core-shell nanocomposite for chemoselective reductions with H_2. Representation of Ag/HT reacting with H_2; both polar and nonpolar hydrogen species are formed. The Ag NPs are covered with a basic material (BM), which reacted with H_2 to result in the exclusive formation of a polar hydrogen species. A basic site of HT and BM is represented by BS. Time course of the reduction of nitrostyrene with H_2 using (**b**) Ag@CeO_2 and (**c**) Ag/CeO_2. Reprinted with permission from Mitsudome *et al.*[97] Copyright 2012 Wiley-VCH.

always higher than 600 °C.[87] With such high working temperatures, the noble metals tend to deactivate through the loss of active surface. The CeO_2-encapsulated noble metal nanocrystal approach offers a powerful tool for minimizing deactivation of the catalyst during the sintering processes.

For instance, in the Pt@CeO_2 multi-core–shell system reported by Zhang and coworker,[75] it was observed that the core–shell nanostructure has much higher thermal stability compared with the simply loaded samples. As shown in Figure 16, after calcinations at 600 °C for 5 h in air, Pt@CeO_2 multi-core–shell hybrid nanospheres maintained their particle size and shape. No obvious growth or aggregation can be observed in the corresponding TEM images. For comparison, the simply mixed Pt–CeO_2 sample exhibited much poorer stability. After the heating treatment, the particles aggregated heavily, and the Pt NPs increased in size from 4 nm to over 20 nm. This result indicates that the core–shell nanostructure can efficiently prevent the mass transformation process at high temperature.

Other types of noble metal@CeO_2 core–shell or yolk–shell hybrid structures also exhibited high thermal stabilities. Moreover, the hybrid nanostructure prepared by fixing the noble metal NPs on the inner walls of hollow CeO_2 supports has been proven to still be effective. As shown in Figures 6d–i, Xia and coworker performed a thermal analysis of the hollow CeO_2 fiber with Pt NPs embedded in the inner faces.[78] The products obtained at 400 and 800 °C still maintained a tubular structure without collapsing, demonstrating a rather high thermal stability for the relatively thin CeO_2 sheath. In addition, the Pt NPs were effectively prevented from aggregating, even with sintering up to 700 °C. However, further increasing the sintering temperature can cause the aggregation of both Pt NPs and CeO_2 sheath.

This result is consistent with our experiment that demonstrated that pure CeO_2 could withstand only calcining temperatures below 700 °C. Higher temperatures could cause an irreversible secondary growth process for CeO_2. Thus, elimination of the protection by CeO_2 could make the noble metals agglomerate. Gorte and coworkers developed a solution to solve the problem: load the monodisperse Pd@CeO_2 core–shell samples onto the secondary supports, including Al_2O_3 and YSZ. The anti-sintering temperature is increased to 850 °C.[89,99]

Activity

Catalytic CO oxidation has been widely investigated as a typical model reaction. Being much different from the previously reported surface-loaded noble metal/metal oxide nanocatalysts with low-temperature CO oxidation capability,[100] the CeO_2-encapsulated noble metal nanocatalysts exhibit much poorer catalytic activities but with markedly increased high-temperature stabilities. For example, Zhang and coworkers developed Pt@CeO_2 multi-core–shell nanostructures for catalytic CO oxidation and compared them with simply mixed Pt–CeO_2 catalysts and pure CeO_2 samples.[75] Their catalytic CO conversion curves are shown in Figure 17. T_{100}, the 100% conversion temperature, has been selected as an important index to evaluate the catalysts' activities. The unheated Pt@CeO_2 sample has the lowest T_{100}, ~140 °C. After calcinations, T_{100} increased slightly, to 145 °C. Simply mixed Pt–CeO_2 has a much higher T_{100}, 170 °C, and after the heat treatment, inactivation was obvious and T_{100} increased to 300 °C. The better catalytic performance of the Pt@CeO_2 sample could be attributed to two factors: the stronger synergistic effect between Pt and CeO_2 caused by the two-face interface redox reaction and the protection of CeO_2 for tiny Pt NPs.

The catalytic methane combustion reaction of Pd@CeO_2/Al_2O_3 nanocatalysts, as compared with Pd/CeO_2 and Pd/CeO_2/Al_2O_3 samples, was studied by Prof. Gorte and demonstrated outstanding catalytic performance.[87] Complete conversion of CH_4 was observed at ~400 °C (Figure 18a). All other reference samples achieved the complete CH_4 conversion above 700 °C. Such an excellent catalytic performance can be attributed to the following three factors: (1) the presence of CeO_2 shifting the temperature window in which the reaction occurs; (2) the protection of the Pd core by the core–shell structure and good contact between Pd and CeO_2 during the high-temperature catalytic reaction; and (3) the effect of the support to enhance the catalytic performance of Pd@CeO_2.

Intriguingly, an energy transfer process is also observed in noble metal@CeO_2 nanostructures, which provides the hybrid sample with high catalytic activity in visible-light photocatalytic reactions. Xu and coworkers compared the visible-light photoactivity with that of traditional Pd/CeO_2 and commercial CeO_2.[87] The peaks in the photoluminescent spectra of the Pd@CeO_2 core–shell nanostructure are much lower than those in the other two samples, indicating the efficiently prolonged lifetime of electron–hole pairs, which is in line with the photocurrent–voltage plots displayed in Figure 19b. Compared with traditional Pd/CeO_2 and commercial CeO_2, the photocurrent density of Pd@CeO_2 is significantly greater, which may be the main reason for the longer life span achieved for the Pd@CeO_2 core–shell sample. Consequently, the photocatalytic activity in the reduction of aromatic nitro compounds follows the order Pd@CeO_2 > supported Pd/CeO_2 > commercial CeO_2.

Selectivity

Selectivity is another important parameter in measuring the quality of a catalyst. Kaneda and coworkers studied the Ag@CeO_2 core–shell nanospheres composed of 10-nm Ag NPs as cores and 3–5-nm CeO_2 assembled outside to form a dense sheath for chemoselective hydrogenation.[96] The nanogaps among the adjacent CeO_2 NPs in the shell permitted the access of reactants to the active Ag sites in the core (Figure 20). Maximizing the interaction between Ag NPs and the basic sites of CeO_2 successfully induced the heterolytic cleavage of H_2 to Ag-hydride and proton species rather than hemolytic cleavage of H_2 on the bare Ag surface of the supported Ag/CeO_2 samples (Figure 13a). Correspondingly, the core–shell nanostructures exhibited an excellent chemoselective reduction of nitrostyrenes, epoxides and unsaturated aldehydes while maintaining the C–C bonds. For instance, the core–shell nanostructures showed high chemoselective conversion (>99%) of 3-nitrostyrene to 3-aminostyrene under high pressure H_2 at 110 °C (Figure 20), excellent activity (98%) and selectivity (>99%) for the catalytic deoxygenation of epoxides to alkenes, and enhanced chemoselective reduction (>99%) of unsaturated aldehydes to the corresponding allylic alcohols. Furthermore, Ag@CeO_2 could be highly dispersed on the CeO_2 matrix, exhibiting catalytic activity six times higher than that of the original Ag@CeO_2 as well as wide applicability for various substrates in the chemoselective reductions of unsaturated aldehydes.

CONCLUSION AND OUTLOOK

Although some encouraging results have been achieved, there remain many challenges. (1) The development of simple and cost-effective synthetic and fabrication processes for CeO_2-encapsulated noble metal nanomaterials is still desirable. (2) To date, besides that for the Pd@CeO_2 system, there has been no report of the successful encapsulation of ultra-small noble metal NPs, especially noble metal nanoclusters (<1 nm) with CeO_2. In general, the catalytic activities of noble metals are highly dependent on their particle sizes. Optimizing the particle sizes of noble metals is an efficient way to increase their catalytic performances.[101] However, the ultra-small particles increase the surface energy, causing the small noble metals to aggregate seriously and thereby interfere with the formation of such core–shell structures. Hence, there is an urgent need to develop new methods to fabricate CeO_2-encapsulated noble metals with controllable particle sizes on the nanoscale. (3) The core materials are still limited to a few noble metals, including Pt, Pd, Au and Ag. The use of other types of noble metals, such as Ir, Ru, Rh and the corresponding noble metal alloys, has yet to be reported. (4) Control of the morphology of both the noble metals and CeO_2 has rarely been reported. It can be predicted that the selectively of special faces of both the noble metals and CeO_2 could greatly increase the hybrids' catalytic activity and selectivity. (5) The hybrid structure, especially the shell thickness in the core–shell or yolk–shell hybrid nanostructures, should be well controlled. It is difficult for some types of substrate molecules to penetrate the thick CeO_2 shell to reach the surface of noble metal cores; however, if the CeO_2 shell is too thin, its protection of the noble metal cores is very limited. The question of how to balance activity and stability is complicated. In our opinion, there are three directions worthy of attention in the future to address this question: (1) vigorously developing seeded growth methods because such a synthetic strategy could ensure control of the size, shape and composition of noble metal cores; (2) introducing an appropriate hard template in the synthesis to produce hollow space in the hybrid nanostructure, which is believed to be an efficient way to optimize the diffusion rate of substrate molecules; (3) quantitatively analyzing the effect of exposed crystal faces of noble metals on CeO_2, which is very helpful for the design of highly active CeO_2-encapsulated noble metal nanocatalysts for special catalytic reactions.

In conclusion, CeO_2-encapsulated noble metal hybrid nanomaterials have exhibited much higher catalytic performance than traditional catalysts. It is believed that in the future, such hybrid nanomaterials will assume a more important role in catalysis, energy conversion, environmental protection and remediation, as well as in the new field of biomedical applications.

CONFLICT OF INTEREST

The authors declare no conflict of interest.

ACKNOWLEDGEMENTS

We are grateful for the financial aid received from the National Natural Science Foundation of China (grant nos. 21221061, 51372242, 91122030 and 21210001), the National Key Basic Research Program of China (no. 2014CB643802) and Jilin Province Youth Foundation (20130522122JH).

1 Max, G., Ataualpa, A. C. B., Agusti, L., Gregori, U. & Feliu, M. Computational perspective on Pd-catalyzed C-C cross-coupling reaction mechanisms. *Acc. Chem. Res.* **46**, 2626–2634 (2013).
2 Zhang, H., Jin, M. S., Xiong, Y. J., Lim, B. & Xia, Y. N. Shape-controlled synthesis of Pd nanocrystals and their catalytic applications. *Acc. Chem. Res.* **46**, 1783–1794 (2013).
3 Jin, M., Zhang, H., Xie, Z. & Xia, Y. Palladium nanocrystals enclosed by {100} and {111} facets in controlled proportions and their catalytic activities for formic acid oxidation. *Energy Environ. Sci* **5**, 6352–6357 (2012).
4 Niu, W., Zhang, L. & Xu, G. Shape-controlled synthesis of single-crystalline palladium nanocrystals. *ACS Nano* **4**, 1987–1996 (2010).
5 Crespo-Quesada, M., Yarulin, A., Jin, M., Xia, Y. & Kiwi-Minsker, L. Structure sensitivity of alkynol hydrogenation on shape- and size-controlled palladium nanocrystals: which sites are most active and selective? *J. Am. Chem. Soc.* **133**, 12787–12794 (2011).
6 Porter, N., Wu, H., Quan, Z. W. & Fang, J. Shape-control and electrocatalytic activity-enhancement of Pt-based bimetallic nanocrystals. *Acc. Chem. Res.* **46**, 1867–1877 (2013).
7 Sun, S., Murray, C. B., Weller, D., Folks, L. & Moser, A. Monodisperse FePt nanoparticles ferromagnetic FePt nanocrystal superlattices. *Science* **287**, 1989–1992 (2000).
8 Yu, T., Kim, D. Y., Zhang, H. & Xia, Y. Platinum concave nanocubes with high-index facets and their enhanced activity for oxygen reduction reaction. *Angew. Chem. Int. Ed.* **50**, 2773–2777 (2011).
9 Wu, Y., Wang, D., Zhou, G., Yu, R., Chen, C. & Li, Y. Sophisticated construction of Au islands on Pt–Ni: an ideal trimetallic nanoframe catalyst. *J. Am. Chem. Soc.* **136**, 11594–11597 (2014).
10 Hong, X., Wang, D., Cai, S., Rong, H. & Li, Y. Single-crystalline octahedral Au–Ag nanoframes. *J. Am. Chem. Soc.* **134**, 18165–18168 (2012).
11 Miyaura, N. & Suzuki, A. Palladium-catalyzed cross-coupling reactions of organoboron compounds. *Chem. Rev.* **95**, 2457–2483 (1995).
12 Jin, M., Zhang, H., Xie, Z. & Xia, Y. Palladium concave nanocubes with high-index facets and their rnhanced catalytic properties. *Angew. Chem. Int. Ed.* **50**, 7850–7854 (2011).
13 Stille, J. K. The palladium-catalyzed cross-coupling reaction of organotin reagents with organic electrophiles. *Angew. Chem. Int. Ed.* **25**, 508–524 (1986).
14 Buchwald, S. L. Cross-coupling (Guest Editorial). *Acc. Chem. Res.* **41**, 1439–1564 (2008).
15 Xue, L. & Lin, Z. Theoretical aspects of palladium-catalysed carbon–carbon cross-coupling reactions. *Chem. Soc. Rev.* **39**, 1692–1705 (2010).
16 Beaumont, S., Kyriakou, G. & Lambert, R. Identity of the active site in gold nanoparticle-catalyzed sonogashira coupling of phenylacetylene and iodobenzene. *J. Am. Chem. Soc.* **132**, 12264–12248 (2010).
17 Zhang, S., Shan, J., Zhu, Y., Frenkel, A., Patlolla, A., Huang, W., Yoon, S., Wang, L., Yoshida, H., Takeda, S. & Tao, F. WGS catalysis and in situ studies of CoO_{1-x}, $PtCo_n/Co_3O_4$, and Pt_mCo_m/CoO_{1-x} nanorod catalysts. *J. Am. Chem. Soc.* **135**, 8283–8293 (2013).
18 An, K., Alayoglu, S., Musselwhite, N., Plamthottam, S., Melaet, G., Lindeman, A. & Somorjai, G. Enhanced CO oxidation rates at the interface of mesoporous oxides and Pt nanoparticles. *J. Am. Chem. Soc.* **135**, 16689–16696 (2013).
19 Guo, S. & Sun, S. FePt nanoparticles assembled on graphene as enhanced catalyst for oxygen reduction reaction. *J. Am. Chem. Soc.* **134**, 2492–2495 (2012).
20 Wang, L., Zhang, S., Zhu, Y., Patlolla, A., Shan, J., Yoshida, H., Takeda, S., Frenkel, A. & Tao, F. Catalysis and *in situ* studies of Rh_1/Co_3O_4 nanorods in reduction of NO with H_2. *ACS Catal* **3**, 1011–1019 (2013).
21 Feng, L., Hoang, D., Tsung, C., Huang, W., Lo, S., Wood, J., Wang, H., Tang, J. & Yang, P. Catalytic properties of Pt cluster-decorated CeO_2 nanostructures. *Nano Res* **4**, 61–71 (2011).
22 Huang, P., Chen, G., Jiang, Z., Jin, R., Zhu, Y. & Sun, Y. Atomically precise Au_{25} superatoms immobilized on CeO_2 nanorods for styrene oxidation. *Nanoscale* **5**, 3668–3672 (2013).
23 Chong, H., Li, P., Xiang, J., Fu, F., Zhang, D., Ran, X. & Zhu, M. Design of an ultrasmall Au nanocluster–CeO_2 mesoporous nanocomposite catalyst for nitrobenzene reduction. *Nanoscale* **5**, 7622–7628 (2013).
24 Cargnello, M., Gentilini, C., Montini, T., Fonda, E., Mehraeen, S., Chi, M., Herrera-Collado, M., Browning, N., Polizzi, S., Pasquato, L. & Fornasiero, P. Active and stable embedded Au@CeO_2 catalysts for preferential oxidation of CO. *Chem. Mater.* **22**, 4335–4345 (2010).
25 Li, B., Gu, T., Ming, T., Wang, J., Wang, P., Wang, J. & Yu, J. (Gold core)@(ceria shell) nanostructures for plasmon-enhanced catalytic reactions under visiblelight. *ACS Nano* **8**, 8152–8162 (2014).
26 Wen, C., Zhu, Y., Ye, Y., Zhang, S., Cheng, F., Liu, Y., Wang, P. & Tao, F. Water–gas shift reaction on metal nanoclusters encapsulated in mesoporous ceria studied with ambient-pressure X-ray photoelectron spectroscopy. *ACS Nano* **6**, 9305–9313 (2012).
27 Lv, X., Zhu, Y., Jiang, H., Zhong, H., Yang, X. & Li, C. Au@TiO_2 double-shelled octahedral nanocages with improved catalytic properties. *Dalton Trans.* **43**, 15111–15118 (2014).
28 Liu, W., Lin, F., Yang, Y., Huang, C., Gwo, S., Huang, M. & Huang, J. The influence of shell thickness of Au@TiO_2 core–shell nanoparticles on the plasmonic enhancement effect in dye-sensitized solar cells. *Nanoscale* **5**, 7953–7962 (2013).
29 Han, L., Zhu, C., Hu, P. & Dong, S. One-pot synthesis of a Au@TiO_2 core–shell nanocomposite and its catalytic property. *RSC Adv* **3**, 12568–12570 (2013).
30 Dillon, R., Joo, J., Zaera, F., Yin, Y. & Bardeen, C. Correlating the excited state relaxation dynamics as measured by photoluminescence and transient absorption with the photocatalytic activity of Au@TiO_2 core–shell nanostructures. *Phys. Chem. Chem. Phys.* **15**, 1488–1496 (2013).
31 Du, J., Qi, J., Wang, D. & Tang, Z. Facile synthesis of Au@TiO_2 core–shell hollow spheres for dye-sensitized solar cells with remarkably improved efficiency. *Energy Environ. Sci.* **5**, 6914–6918 (2012).
32 Seh, Z., Liu, S., Zhang, S., Shah, K. & Han, M. Synthesis and multiple reuse of eccentric Au@TiO_2 nanostructures as catalysts. *Chem. Commun.* **47**, 6689–6691 (2011).
33 Xiong, Z., Zhang, L. & Zhao, X. S. One-step synthesis of metal@titania core–shell materials for visible-light photocatalysis and catalytic reduction reaction. *Chem. Eur. J* **20**, 1–7 (2014).
34 Lee, I., Joo, J., Yin, Y. & Zaera, F. A yolk-shell nanoarchitecture for Au/TiO_2 catalysts. *Angew. Chem. Int. Ed.* **50**, 10208–10211 (2011).
35 Lekeufack, D., Brioude, A., Mouti, A., Alauzun, J., Stadelmann, P., Coleman, A. & Miele, P. Core–shell Au@(TiO_2, SiO_2) nanoparticles with tunable morphology. *Chem. Commun.* **46**, 4544–4546 (2010).
36 Dahlberg, K. & Schwank, J. Synthesis of Ni@SiO_2 nanotube particles in a water-in-oil microemulsion template. *Chem. Mater.* **24**: 2635–2644 (2012).
37 Li, Z., Mo, L., Kathiraser, Y. & Kawi, S. Yolk–satellite–shell structured Ni–yolk@Ni@-SiO_2 nanocomposite: superb catalyst toward Methane CO_2 reforming reaction. *ACS Catal* **4**, 1526–1536 (2014).
38 Park, J., Lee, H., Kim, J., Park, K. & Song, H. Catalytic hydrogen transfer of ketones over Ni@SiO_2 yolk – shell nanocatalysts with tiny metal cores. *J. Phys. Chem. C* **114**, 6381–6388 (2010).
39 DuChene, J., Almeida, R. & Wei, W. Facile synthesis of anisotropic Au@SiO_2 core–shell nanostructures. *Dalton Trans.* **2012**, 7879–7882 (2012).
40 Güttel, R., Paul, M. & Schüth, F. Ex-post size control of high-temperature-stable yolk–shell Au, @ZrO_2 catalysts. *Chem. Commun.* **46**, 895–897 (2010).
41 Nair, A., Pradeep, T. & MacLaren, I. An investigation of the structure of stearate monolayers on Au@ZrO_2 and Ag@ZrO_2 core–shell nanoparticles. *J. Mater. Chem.* **14**, 857–862 (2004).
42 Sun, C., Li, H. & Chen, L. Nanostructured ceria-based materials: synthesis, properties, and applications. *Energy Environ. Sci* **5**, 8475–8505 (2012).
43 Kaspar, J., Fornasiero, P. & Graziani, M. Use of CeO_2-based oxides in the three-way catalysis. *Catal. Today* **2**, 285–298 (1999).
44 Fu, Q., Weber, A. & Flytzani-Stephanopoulo, M. Nanostructured Au–CeO_2 catalysts for low-temperature water–gas shift. *Catal. Lett.* **77**, 87–95 (2001).
45 Fu, Q., Saltsburg, H. & Flytzani-Stephanopoulo, M. Active nonmetallic Au and Pt species on ceria-based water–gas shift catalysts. *Science* **301**, 935–938 (2003).
46 Beie, H. & Gnorich, A. Oxygen gas sensors based on CeO_2 thick and thin films. *Sens. Actuat. B* **4**, 393–399 (1991).
47 Jasinski, P., Suzuki, T. & Anderson, H. Nanocrystalline undoped ceria oxygen sensor. *Sens. Actuat. B* **95**, 73–77 (2003).
48 Wang, L., Huang, H., Xiao, S., Cai, D., Liu, Y., Liu, B., Wang, D., Wang, C., Li, H., Wang, Y., Li, Q. & Wang, T. Enhanced sensitivity and stability of room-temperature NH_3 sensors using core – shell CeO_2 nanoparticles@cross-linked PANI with p – n heterojunctions. *ACS Appl. Mater. Interfaces* **6**, 14131–14140 (2014).
49 Stoukides, M. Solid-electrolyte membrane reactors: current experience and future outlook. *Catal. Rev. Sci. Eng.* **42**, 1–70 (2000).
50 Chu, Y., Wang, Z., Jiang, Z., Gu, D. & Yin, G. A novel structural design of a Pt/C-CeO_2 catalyst with improved performance for methanol electro-oxidation by β-cyclodextrin carbonization. *Adv. Mater.* **23**, 3100–3104 (2011).
51 Chu, Y., Cao, J., Daia, Z. & Tan, X. A novel Pt/CeO_2 catalyst coated with nitrogen-doped carbon with excellent performance for DMFCs. *J. Mater. Chem. A* **2**, 4038–4044 (2014).

52 Cao, M., Wu, D. & Cao, R. Recent advances in the stabilization of platinum electrocatalysts for fuel-cell reactions. *ChemCatChem* **6**, 26–45 (2014).
53 Li, G., Lu, F., Wei, X., Song, X., Sun, Z., Yang, Z. & Yang, S. Nanoporous Ag–CeO_2 ribbons prepared by chemical dealloying and their electrocatalytic properties. *J. Mater. Chem. A* **1**, 4974–4981 (2013).
54 Wang, X., Li, X., Liu, D., Song, S. & Zhang, H. Green synthesis of Pt/CeO_2/graphene hybrid nanomaterials with remarkably enhanced electrocatalytic properties. *Chem. Commun.* **48**, 2885–2887 (2012).
55 Menéndez, C., Zhou, Y., Marin, C., Lawrence, N., Coughlin, E., Cheung, C. & Cabrera, C. Preparation and characterization of Pt/Pt:CeO_{2-x} nanorod catalysts for short chain alcohol electrooxidation in alkaline media. *RSC Adv* **4**, 33489–33496 (2014).
56 Shen, Z., Liu, J., Hu, F., Liu, S., Cao, N., Sui, Y., Zeng, Q. & Shen, Y. Bottom-up synthesis of cerium–citric acid coordination polymers hollow microspheres with tunable shell thickness and their corresponding porous CeO_2 hollow spheres for Pt-based electrocatalysts. *CrystEngComm* **16**, 3387–3394 (2014).
57 Gao, Y., Wang, W., Chang, S. & Huang, W. Morphology effect of CeO_2 support in the preparation, metal–support interaction, and catalytic performance of Pt/CeO_2 catalysts. *ChemCatChem* **5**, 3610–3620 (2013).
58 Yi, N., Si, R., Saltsburg, H. & Flytzani-Stephanopoulos, M. Active gold species on cerium oxide nanoshapes for methanol steam reforming and the watergas shift reactions. *Energy Environ. Sci* **3**, 831–837 (2010).
59 Zhou, H., Wu, H., Shen, J., Yin, A., Sun, L. & Yan, C. Thermally stable Pt/CeO_2 heteronanocomposites with high catalytic activity. *J. Am. Chem. Soc.* **132**, 4998–4999 (2010).
60 Li, X., Wang, X., Liu, D., Song, S. & Zhang, H. Multifunctional nanostructures based on porous silica covered Fe_3O_4@CeO_2–Pt composites: a thermally stable and magnetically-recyclable catalyst system. *Chem. Commun.* **50**, 7198–7201 (2014).
61 Wang, X., Liu, D., Song, S. & Zhang, H. Synthesis of highly active Pt–CeO_2 hybrids with tunable secondary nanostructures for the catalytic hydrolysis of ammonia borane. *Chem. Commun.* **48**, 10207–10209 (2012).
62 Wang, X., Liu, D., Song, S. & Zhang, H. Graphene oxide induced formation of Pt–CeO_2 hybrid nanoflowers with tunable CeO_2 thickness for catalytic hydrolysis of ammonia borane. *Chem. Eur. J* **19**, 8082–8086 (2013).
63 Lin, J., Li, L., Huang, Y., Zhang, W., Wang, X., Wang, A. & Zhang, T. *In situ* calorimetric study: structural effects on adsorption and catalytic performances for CO oxidation over Ir-in-CeO_2 and Ir-on-CeO_2 catalysts. *J. Phys. Chem. C* **115**, 16509–16517 (2011).
64 Yu, K., Wu, Z., Zhao, Q., Li, B. & Xie, Y. High-temperature-stable Au@SnO_2 core/shell supported catalyst for CO oxidation. *J. Phys. Chem. C* **112**: pp 2244–2247 (2008).
65 Oldfield, G., Ung, T. & Mulvaney, P. Au@SnO_2 core–shell nanocapacitors. *Adv. Mater.* **12**, 1519–1522 (2000).
66 Wang, L., Dou, H., Lou, Z. & Zhang, T. Encapsuled nanoreactors (Au@SnO_2): a new sensing material for chemical sensors. *Nanoscale* **5**, 2686–2691 (2013).
67 Kuo, C., Hua, T. & Huang, M. Au Nanocrystal-directed growth of Au – Cu_2O core – shell heterostructures with precise morphological control. *J. Am. Chem. Soc.* **131**, 17871–17878 (2009).
68 Jiang, D., Zhou, W., Zhong, X., Zhang, Y. & Li, X. Distinguishing localized surface plasmon resonance and schottky junction of Au–Cu_2O composites by their molecular spacer dependence. *ACS Appl. Mater. Interfaces* **6**, 10958–10962 (2014).
69 Wang, W., Lyu, L. & Huang, M. Investigation of the effects of polyhedral gold nanocrystal morphology and facets on the formation of Au–Cu_2O core–shell heterostructures. *Chem. Mater.* **23**, 2677–2684 (2011).
70 Zhang, L., Blom, D. & Wang, H. Au–Cu_2O core–shell nanoparticles: a hybrid metal-semiconductor heteronanostructure with geometrically tunable optical properties. *Chem. Mater.* **23**, 4587–4598 (2011).
71 Liu, D., Ding, S., Lin, H., Liu, B., Ye, Z., Fan, F., Ren, B. & Tian, Z. Distinctive enhanced and tunable plasmon resonant absorption from controllable Au@Cu_2O nanoparticles: experimental and theoretical modeling. *J. Phys. Chem. C* **116**, 4477–4483 (2012).
72 Li, J., Cushing, S., Bright, J., Meng, F., Senty, T., Zheng, P., Bristow, A. & Wu, N. Ag@Cu_2O core-shell nanoparticles as visible-light plasmonic photocatalysts. *ACS Catal* **3**, 47–51 (2013).
73 Sun, H., He, J., Wang, J., Zhang, S., Liu, C., Sritharan, T., Mhaisalkar, S., Han, M., Wang, D. & Chen, H. Investigating the multiple roles of polyvinylpyrrolidone for a general methodology of oxide encapsulation. *J. Am. Chem. Soc.* **135**, 9099–9110 (2013).
74 Li, G. & Tang, Z. Noble metal nanoparticle@metal oxide core/yolk–shell nanostructures as catalysts: recent progress and perspective. *Nanoscale* **6**, 3995–4011 (2014).
75 Casavola, M., Buonsanti, R., Caputo, G. & Cozzoli, P. Colloidal strategies for preparing oxide-based hybrid nanocrystals. *Eur. J. Inorg. Chem.* **8**, 837–854 (2008).
76 Yu, T., Zeng, J., Lim, B. & Xia, Y. Aqueous-phase synthesis of Pt/CeO_2 hybrid nanostructures and their catalytic properties. *Adv. Mater.* **22**, 5188–5192 (2010).
77 Zhang, N., Fu, X. & Xu, Y. A facile and green approach to synthesize Pt@CeO_2 nanocomposite with tunable core-shell and yolk-shell structure and its application as a visible light photocatalyst. *J. Mater. Chem.* **21**, 8152–8158 (2011).
78 Wang, X., Liu, D., Song, S. & Zhang, H. Pt@CeO_2 multi-core@shell self-assembled nanospheres: clean synthesis, structure optimization, and catalytic applications. *J. Am. Chem. Soc.* **135**, 15864–15872 (2013).
79 Yang, P., Zhao, D., Margolese, D., Chmelka, B. & Stucky, G. Generalized syntheses of large-pore mesoporous metal oxides with semicrystalline frameworks. *Nature* **396**, 152–155 (1998).
80 Yang, P., Deng, T., Zhao, D., Feng, P., Pine, D., Chmelka, B., Whitesides, G. & Stucky, G. Hierarchically Ordered Oxides. *Science* **282**, 2244–2246 (1998).
81 Shi, Y., Guo, B., Corr, S., Shi, Q., Hu, Y., Heier, K., Chen, L., Seshadri, R. & Stucky, G. Ordered Mesoporous Metallic MoO_2 Materials with Highly Reversible Lithium Storage Capacity. *Nano Lett.* **9**, 4215–4220 (2009).
82 Lu, A. & Schüth, F. Nanocasting: a versatile strategy for creating nanostructured porous materials. *Adv. Mater* **18**, 1793–1805 (2006).
83 Chen, C., Nan, C., Wang, D., Su, Q., Duan, H., Liu, X., Zhang, L., Chu, D., Song, W., Peng, Q. & Li, Y. Mesoporous multicomponent nanocomposite colloidal spheres: ideal high-temperature stable model catalysts. *Angew. Chem. Int. Ed.* **50**, 3725–3729 (2011).
84 Concepcion, P., Corma, A., Silvestre-Albero, J., Franco, V. & Chane-Ching, J. Chemoselective hydrogenation catalysts: Pt on mesostructured CeO_2 nanoparticles embedded within ultrathin layers of SiO_2 binder. *J. Am. Chem. Soc.* **126**, 5523–5532 (2004).
85 Yoon, K., Yang, Y., Lu, P., Peng, H., Masias, K., Fanson, P., Campbell, C. & Xia, Y. A highly reactive and sinter-resistant catalytic system based on Platinum nanoparticles embedded in the inner surfaces of CeO_2 hollow fibers. *Angew. Chem. Int. Ed.* **51**, 9543–9546 (2012).
86 Cargnello, M., Jaén, J., Garrido, J., Bakhmutsky, K., Montini, T., Gámez, J., Gorte, R. & Fornasiero, P. Exceptional activity for methane combustion over modular Pd@CeO_2 subunits on functionalized Al_2O_3. *Science* **337**, 713–717 (2012).
87 Cargnello, M., Wieder, N., Montini, T., Gorte, R. & Fornasiero, P. Synthesis of dispersible Pd@CeO_2 core-shell nanostructures by self-assembly. *J. Am. Chem. Soc.* **132**, 1402–1409 (2010).
88 Wieder, N., Cargnello, M., Bakhmutsky, K., Montini, T., Fornasiero, P. & Gorte, R. Study of the water-gas-shift reaction on Pd@CeO_2/Al_2O_3 core – shell catalysts. *J. Phys. Chem. C* **115**, 915–919 (2011).
89 Adijanto, L., Sampath, A., Yu, A., Cargnello, M., Fornasiero, P., Gorte, R. & Vohs, J. Synthesis and stability of Pd@CeO_2 core–shell catalyst films in solid oxide fuel cell anodes. *ACS Catal* **3**, 1801–1809 (2013).
90 Adijanto, L., Bennett, D., Chen, C., Yu, A., Cargnello, M., Fornasiero, P., Gorte, R. & Vohs, J. Exceptional thermal stability of Pd@CeO_2 core–shell catalyst nanostructures grafted onto an oxide surface. *Nano Lett.* **13**, 2252–2257 (2013).
91 Zhang, N., Liu, S., Fu, X. & Xu, Y. A simple strategy for fabrication of 'plum-pudding' type Pd@CeO_2 semiconductor nanocomposite as a visible-light-driven photocatalyst for selective pxidation. *J. Phys. Chem. C* **115**, 22901–22909 (2011).
92 Chen, C., Fang, X., Wu, B., Huang, L. & Zheng, N. A multi-yolk-shell structured nanocatalyst containing sub-10 nm Pd nanoparticles in porous CeO_2. *ChemCatChem* **4**, 1–10 (2012).
93 Zhang, N. & Xu, Y. Aggregation- and leaching-resistant, reusable, and multifunctional Pd@CeO_2 as a robust nanocatalyst achieved by a hollow core – shell strategy. *Chem. Mater.* **25**, 1979–1988 (2013).
94 Qi, J., Chen, J., Li, G., Li, S., Gao, Y. & Tang, Z. Facile synthesis of core–shell Au@CeO_2 nanocomposites with remarkablyenhanced catalytic activity for CO oxidation. *Energy Environ. Sci* **5**, 8937–8941 (2012).
95 Kayama, T., Yamazaki, K. & Shinjoh, H. Nanostructured ceria – silver synthesized in a one-pot redox reaction catalyzes carbon oxidation. *J. Am. Chem. Soc.* **132**, 13154–13155 (2010).
96 Zhang, J., Li, L., Huang, X. & Li, G. Fabrication of Ag–CeO_2 core–shell nanospheres with enhanced catalytic performance due to strengthening of the interfacial interactions. *J. Mater. Chem.* **22**, 10480–10487 (2012).
97 Mitsudome, T., Mikami, Y., Matoba, M., Mizugaki, T., Jitsukawa, K. & Kaneda, K. Design of a silver–cerium dioxide core–shell nanocomposite catalyst for chemoselective reduction reactions. *Angew. Chem. Int. Ed.* **51**, 136–139 (2012).
98 Liu, B., Yu, S., Wang, Q., Hu, W., Jing, P., Liu, Y., Jia, W., Liu, Y., Liu, L. & Zhang, J. Hollow mesoporous ceria nanoreactors with enhanced activity and stability for catalytic application. *Chem. Comm* **49**, 3757–3759 (2013).
99 Wang, X., Liu, D., Song, S., Zeng, L. & Zhang, Y. Water-soluble Au–CeO_2 hybrid nanosheets with high catalytic activity and recyclability. *Dalton Trans.* **41**, 7193–7195 (2012).
100 Jia, C., Liu, Y., Bongard, H. & Schüth, F. Very low temperature CO oxidation over colloidally deposited gold nanoparticles on $Mg(OH)_2$ and MgO. *J. Am. Chem. Soc.* **132**, 1520–1522 (2010).
101 Herzing, A., Kiely, C., Carley, A., Landon, P. & Hutchings, G. Identification of active gold nanoclusters on iron oxide supports for CO oxidation. *Science* **321**, 1331–1335 (2008).

Shuyan Song received his BSc degree in chemistry in 2003 and his MSc in inorganic chemistry in 2006, both from Northeast Normal University. He joined the group led by Prof. Hongjie Zhang at Changchun Institute of Applied Chemistry, Chinese Academy of Sciences (CAS), where he received his PhD in inorganic chemistry in 2009. He is working as an associate professor under the direction of Prof. Zhang at Changchun Institute of Applied Chemistry, CAS. His current research focuses on functional lanthanide nanomaterials.

Xiao Wang joined the group led by Prof. Hongjie Zhang at Changchun Institute of Applied Chemistry, Chinese Academy of Sciences (CAS), where he received his PhD in inorganic chemistry in 2013. He is working as a Research Assistant under the direction of Prof. Zhang at Changchun Institute of Applied Chemistry, CAS. His current research focuses on the synthesis and catalytic application of CeO_2-based noble metal nanocatalysts.

Hongjie Zhang received his BS (1978) from Peking University and his MS (1985) from Changchun Institute of Applied Chemistry, Chinese Academy of Sciences in China. He studied solid-state chemistry at the University of Bordeaux I (France) and received a PhD from that university in 1993. In 1985, he joined the Changchun Institute of Applied Chemistry, Chinese Academy of Sciences, as a research assistant, and he was promoted to a full professor in 1994. His current research focuses on the development and application of advanced functional lanthanide materials.